Check for updates

JOURNAL OF QUATERNARY SCIENCE (2024) **39**(6) 890–904 ISSN 0267-8179. DOI: 10.1002/jqs.3647

JQS Journal of Quaternary Science QRA Quaternary Research Association

Marine and terrestrial environmental change during the MIS 5–4 transition (southern North Sea area)

IRENE M. WAAJEN,[1,2]* FRANCIEN PETERSE,[1] FRANK P. WESSELINGH,[1,3] FREEK S. BUSSCHERS,[2] FRIEDERIKE WAGNER-CREMER,[1] SYTZE VAN HETEREN[2] and TIMME H. DONDERS[1]

[1]Faculty of Geosciences, Utrecht University, Utrecht, the Netherlands
[2]TNO – Geological Survey of the Netherlands, Utrecht, the Netherlands
[3]Naturalis Biodiversity Center, Leiden, The Netherlands

Received 14 March 2024; Revised 10 June 2024; Accepted 1 July 2024

ABSTRACT: The Late Pleistocene Marine Isotope Stage (MIS) 5 – MIS 4 transition (at ca. 75 ka) is globally known to correspond to a period of strong cooling and sea-level lowering. Terrestrial records indicate the transition had a large impact on terrestrial environments, but the impact on coastal and shallow-marine areas is poorly documented due to a lack of well-dated, continuous archives caused by erosion during succeeding glacial lowstands. The extensive offshore deposits of the Brown Bank Formation in the southern North Sea yield a valuable record of this transition in a shallow-marine environment. We show that the southern North Sea experienced subarctic marine conditions with a high input of terrestrial material during the MIS 5–4 transition. These continued marine conditions, which have not been described earlier for northwestern Europe, show that sea level remained relatively high, and lagged cooling on land inferred from lipid-biomarker palaeothermometry. The time-lag between terrestrial cooling and sea-level fall created a sediment preservation window during the onset of MIS 4 in a shallow-marine environment. Our record captures changes in both the terrestrial and shallow-marine environments, and allows for linking terrestrial and marine records of the MIS 5–4 transition in NW Europe.
© 2024 The Author(s). *Journal of Quaternary Science* Published by John Wiley & Sons Ltd.

KEYWORDS: Brown Bank; environmental change; Marine Isotope Stages 5 and 4; North Sea; palaeoclimate

Introduction

Depositional records of major cooling transitions in coastal and shallow-marine areas are commonly removed by erosion during succeeding glacial lowstands, creating a bias in our understanding of landscape and biotic response to rapid climate change. However, these coastal and shallow-marine areas are the regions where large and rapid climate change can radically change landscapes. In particular, shifting coastlines affect basin shape, salinity regimes, river courses and biota. This situation also applies to the transition from Marine Isotope Stage (MIS) 5 to MIS 4 (80–70 ka), which is one of the strongest cooling phases of the last glacial cycle. The transition is mainly known from lacustrine, polar ice-core or distal oceanic records, while published continuous and dating records from shallow-marine and coastal environments are absent to our knowledge.

MIS 5 is subdivided into five sub-stages, MIS 5e–5a. Following the Last Interglacial stage MIS 5e (ca. 130–115 ka), the subsequent substages 5d–5a (ca. 115–72 ka) represent the Early Weichselian (Brauer et al., 2007; Shackleton, 1969; Shackleton et al., 2003; Sier et al., 2011). The MIS 5e–5a succession represents a complex, step-wise transition from the warm Eemian interglacial into the last glacial period. In northwestern Europe, the final Early Weichselian substage MIS 5a (ca. 84–72 ka) was marked by temperate, interstadial climate conditions (e.g. Behre et al., 2005; Behre, 1989; Müller & Sánchez Goñi, 2007; Sánchez Goñi et al., 2013). Here we apply the interpretation that the first half of MIS 5a corresponds in western Europe to the Odderade/St. Germain interstadial, where the end of MIS 5a, after 78 ka, is referred to as the MIS 5–4 transition (Fig. 1) (Sánchez Goñi et al., 2013; Wohlfarth, 2013).

The transition into MIS 4 was characterized by a decrease in Northern Hemisphere (NH) summer insolation, global climate cooling, rapid growth of continental ice sheets, abrupt sea-level fall and a sudden drop in atmospheric CO_2 (Berger, 1978; McManus et al., 1994; Sánchez Goñi et al., 2013). Major ice expansion in the NH during the first half of MIS 4 (ca. 72–65 ka) resulted in an NH ice limit that was close to the maximum ice extent of the Last Glacial Maximum (LGM, MIS 2), although with different configurations (Batchelor et al., 2019; Dalton et al., 2022; Ruddiman & McIntyre, 1981; Toucanne et al., 2023). Global sea levels dropped as water was captured in growing polar ice caps. Although the exact timing and height of global sea-level trajectories has been discussed, the drop in eustatic sea level between the MIS 5a highstand (ca. 83–77 ka) and MIS 4 lowstand (ca. 67–60 ka) is estimated between 45 and 65 m (Gowan et al., 2021; Pico et al., 2017; Spratt & Lisiecki, 2016; Waelbroeck et al., 2002). During the MIS 5–4 transition, a succession of short, temperate interstadials and cold stadials affected climate. They are recorded by the two largest $\delta^{18}O$ shifts in the North Greenland Ice Core Project (NGRIP) oxygen isotope record of the last glacial cycle, the Greenland Stadials (GS) and Interstadials (GI) 20 and 19 (Fig. 1; NGRIP Members, 2004). The end of GI 19 is characterized by a rapid lowering of $\delta^{18}O$, caused by the stronger glacial conditions and increase in continental ice cover during MIS 4.

In Europe, the biotic response to the cooling of the MIS 5–4 transition has been studied in lacustrine and deep-marine

*Correspondence: Irene M. Waajen, as above.
E-mail: irene.waajen@tno.nl

© 2024 The Author(s). *Journal of Quaternary Science* Published by John Wiley & Sons Ltd.
This is an open access article under the terms of the Creative Commons Attribution-NonCommercial License, which permits use, distribution and reproduction in any medium, provided the original work is properly cited and is not used for commercial purposes.

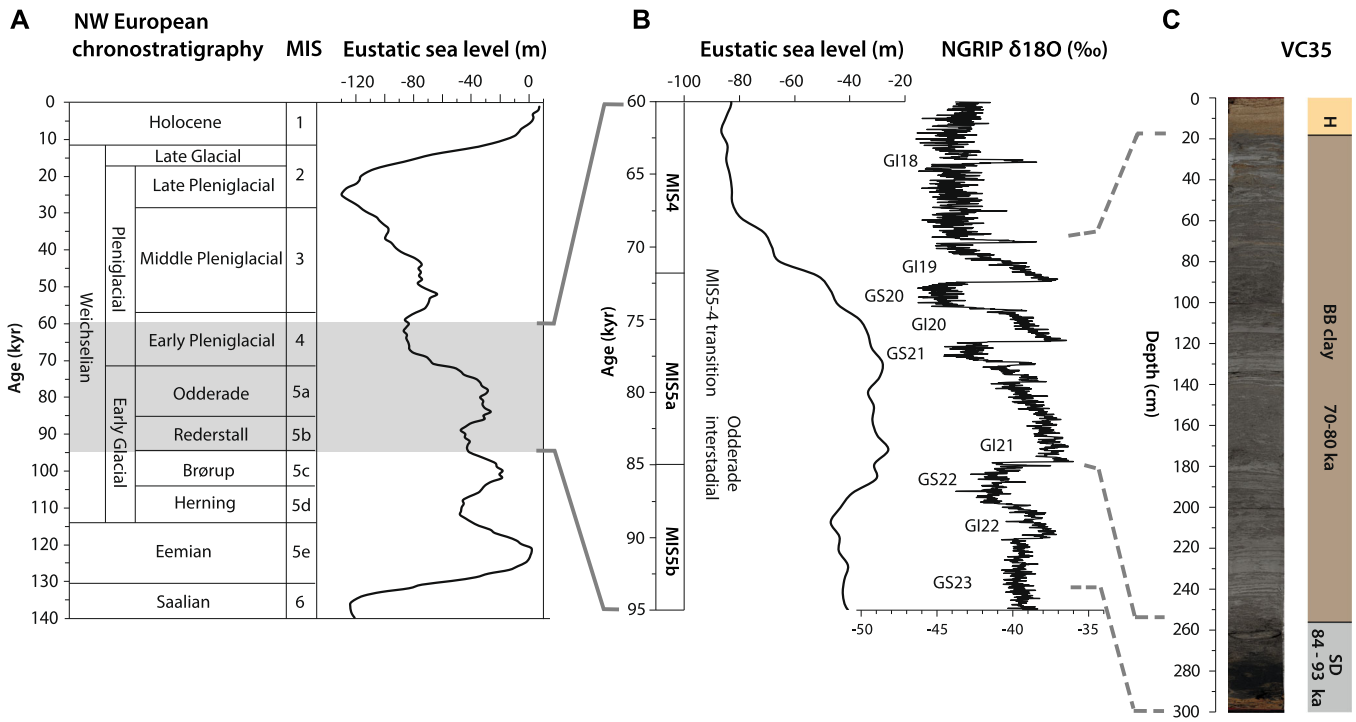

Figure 1. (A) NW European chronostratigraphy over the last glacial cycle, including marine isotope stages (Lisiecki & Raymo, 2005) and eustatic sea level curve (Spratt & Lisiecki, 2016). (B) Insert zooming in on the MIS 5–4 transition, including NGRIP oxygen isotope record GICC05modelext (North Greenland Ice Core Project (NGRIP) Members, 2004; Wolff et al., 2010) with Greenland Stadials (GS) and Greenland Interstadials (GI). (C) Core photo of VC35, with basic stratigraphic units (SD = sand dune unit; BB = Brown Bank clay unit; H = Holocene sand unit) and their age range (including uncertainty of OSL dates; Waajen et al., 2024). [Color figure can be viewed at wileyonlinelibrary.com]

sedimentary records. Before this climate deterioration set in, western Europe was covered by temperate interstadial vegetation (St. Germain II/Odderade interstadial, related to MIS 5a; e.g. Wohlfarth, 2013). The relatively warm, interstadial conditions had a shorter duration in northern Europe than in southern Europe (Wohlfarth, 2013). In southern Europe an additional short interstadial occurred at the final phase of MIS 5a (Müller & Sánchez Goñi, 2007; Sánchez Goñi et al., 2005; Shackleton et al., 2003). Early MIS 4 pollen records throughout western Europe are characterized by a decrease in arboreal pollen, whereas in northern sites forests were completely replaced by a steppe–tundra vegetation (e.g. Behre, 1989). Records from the Bay of Biscay show a decoupling between temperature changes in western Europe and in the Atlantic ocean during the MIS 5–4 transition, with temperate forests being replaced by boreal forests during intervals of warming in eastern North Atlantic ocean waters, and vice versa. Peaks in western European temperate forest cover, however, were synchronous with maxima in eastern North Atlantic Ocean temperatures (Sánchez Goñi et al., 2013). The southernmost evidence for this decoupling phenomenon comes from around 42° N, but the northward extent has not yet been constrained.

The southern North Sea basin holds records covering the MIS 5 – MIS 4 transition, documented in the Brown Bank Formation (BB Fm; Waajen et al., 2024). As the southern North Sea is a relatively flat, shallow shelf sea, it is sensitive to minor climate and sea-level variations. Owing to the drainage of multiple major rivers, the sedimentary record of the southern North Sea contains an imprint of both terrestrial and marine signals. During most of MIS 4, the southern North Sea was dry land with fluvial systems eroding parts of previously deposited marine sediments (Busschers et al., 2007; Törnqvist et al., 2000). The British–Irish ice sheet (BIIS) and Fennoscandian Ice Sheet (FIS) probably did not merge during MIS 4, providing a potential northern drainage route for NW European rivers (Toucanne et al., 2023).

We target the BB Fm to produce a new integrated palaeoenvironment and palaeoclimate framework for the transition from MIS 5 to MIS 4 and show biotic and abiotic environmental response to rapid cooling in a shallow-marine area. We analyse both marine and terrestrial biotic and abiotic environmental proxies on previously optically stimulated luminescence (OSL)-dated cores from the BB Fm (Waajen et al., 2024) to reconstruct the marine environment (including salinity), terrestrial input and the vegetation of the hinterland. This study also provides the first reconstruction of Early Weichselian air temperature for the North Sea region, using temperature-sensitive branched glycerol dialkyl glycerol tetraethers (GDGTs; Dearing Crampton-Flood et al., 2020; Weijers et al., 2007) and pollen-based transfer functions (Chevalier et al., 2020). Our new palaeoenvironmental and palaeoclimatic framework fills an important gap between the existing local terrestrial and distal oceanic records and highlights the little-studied response of shallow-marine and coastal landscape to climatic cooling.

Brown Bank Formation and site description

The depositional setting of the BB Fm was previously interpreted as either freshwater dominated (Oele, 1971), or transitional from brackish lagoonal to freshwater (Cameron et al., 1989; Zagwijn, 1983). More recently, it has been interpreted to represent a shallow-marine depositional setting with high terrestrial input (Eaton et al., 2020; Laban, 1995; Waajen et al., 2024). Several depositional phases in the BB Fm are distinguished on 2D high-resolution seismic profiles (Eaton et al., 2020; Missiaen et al., 2021, Waajen et al., 2024). Initially, pollen studies suggested deposition occurred around late MIS 5e and MIS 5d (Laban & Mesdag, 1995; Zagwijn, 1983), while luminescence ages from vibrocores show a range between 85 and 55 ka, corresponding to MIS 5a

© 2024 The Author(s). *Journal of Quaternary Science* Published by John Wiley & Sons Ltd.

– MIS 3 (Limpenny et al., 2011; Wessex Archaeology, 2018, Waajen et al., 2024). Recent dating of the BB Fm from a set of cores east of the Brown Bank ridge, at the flank of the tidal scour 'Het Gat' (site FG; Fig. 2), and thorough assessment of saturation criteria, show ages indicative for the MIS 5–4 transition (ca. 80–70 ka; Waajen et al., 2024).

Site FG is located 83 km offshore the modern Dutch coastline and is ca. 125 km south of the southernmost ice limit during the LGM. At this location, a combination of 2D acoustic reflection profiles and sedimentological and chronological analyses have been performed on three vibrocores (VC34, VC35 and VC36, Fig. 2b, Table 1). Vibrocores VC35 and VC36 are used for this study. In summary, the cores reveal a transition from a submarine dune system, resembling high-energy deposition (BB Fm, SD unit, ca. 93–84 ka based on OSL), into a low-energy, laminated silty clay unit, which includes sandy intervals (BB Fm, Clay unit, ca. 80–70 ka based on OSL and pollen biostratigraphy; Waajen et al., 2024). This clay unit at site FG is truncated and overlain by 12–20 cm of Holocene marine sands. Sedimentary characteristics, organic matter (OM) content, elemental composition, and an age assessment based on luminescence dating and pollen biostratigraphy are presented in Waajen et al. (2024), and forms the basis for the current study on developing a palaeoenvironmental and palaeoclimatic framework of the MIS 5–4 transition in the southern North Sea.

Methodology

Sediment cores

The three vibrocores, VC34, VC35 and VC36, were taken by a Marine Sampling Holland electrical vibrocorer onboard RV

Table 1. Location of the vibrocores used in this study and described by Waajen et al. (2024).

Core no.	Coordinates (WGS84-UTM31N)	Core depth (cm)	Water depth (m MSL)	Number GSN
VC34	523775, 5827987	266	39.28	BP080111
VC35	523766, 5827951	300	39.83	BP080094
VC36	523757, 5827950	305	39.78	BP080095

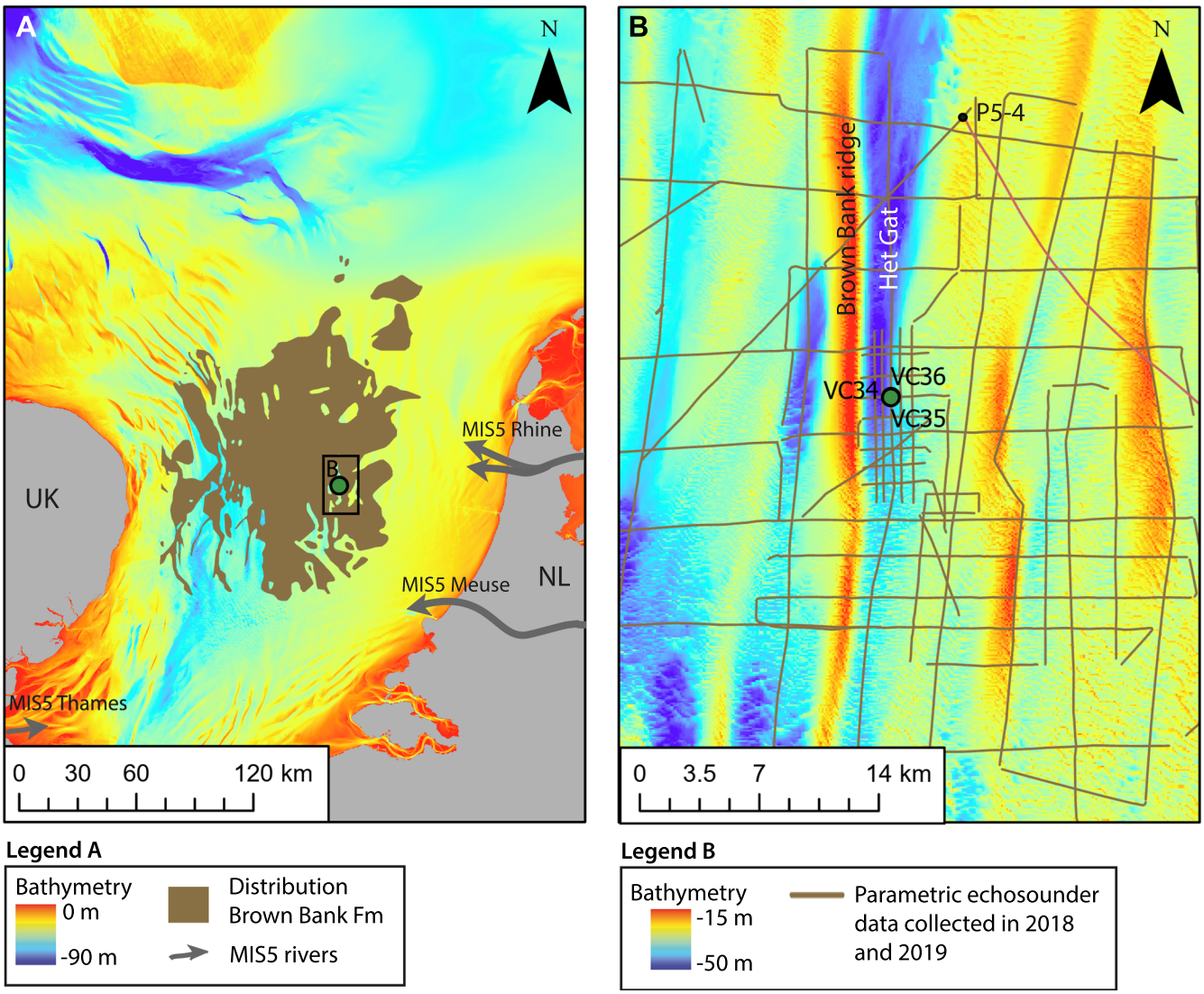

Figure 2. (A) Bathymetric map of the southern North Sea (EMODnet Bathymetry Consortium, 2020) with the distribution of the BB Fm mapped by Cameron et al. (1989). The locations of the main rivers in the area during MIS 5 are also indicated (based on Hijma et al., 2012). (B) Vibrocore locations at the flank of 'Het Gat', where cores VC34, VC35 and VC36 were obtained close together. The location of borehole P5-4 (Zagwijn, 1983) is also indicated. Adapted from Waajen et al. (2024). [Color figure can be viewed at wileyonlinelibrary.com]

© 2024 The Author(s). *Journal of Quaternary Science* Published by John Wiley & Sons Ltd.

Pelagia (cruise 64PE439, 2018). On board RV *Pelagia* an echosounder was used to determine the water depth relative to mean sea level (MSL), which was corrected for tidal fluctuations using a tidal model of the North Sea (Deltares). The three vibrocores were collected within 40 m of each other (Fig. 1B) in order to capture the same approximate succession. Descriptions of the three cores can be found in the Supporting Information, including estimations of lutum, silt and sand content for VC35 and VC36, based on sediment characteristics and visual comparison to measured samples under a microscope. Simplified logs can be viewed in the DINOloket database (www.dinoloket.nl/en) of the Geological Survey of the Netherlands (GSN), using the numbers in the right column of Table 1. Cores VC35 and VC36, used for this study, were photographed and logged at the GSN, where they remain stored.

Diatom analysis

Diatoms are unicellular siliceous microalgae found in most fresh- and saltwater environments, and their assemblages provide information on the aquatic environment, such as salinity. For diatom preparation, mineral residues (density $>2.0\,g\,cm^{-3}$) were used from ten samples, previously processed for pollen analyses within the BB clay unit of core VC35 (pollen preparations steps are described in Waajen et al., 2024). Sample depths are noted in the Supporting Information. Diatoms in these residues were separated from minerals by heavy liquid flotation over sodium polytungstate at a density of $2.3\,g\,cm^{-3}$. The diatom samples were mounted on slides using Zyrax and analysed under transmitted light. Environmental interpretations of diatoms were based on indices by Dam et al. (1994) and Vos & Wolf (1993), complemented with taxonomical insights from others (e.g. Denys, 1991; Ziemann, 1971). Diatom counts are expressed as percentage abundances and separated into ecological groups.

Mollusc analysis

Mollusc shells can provide strong palaeoenvironmental insights. Whole molluscs and fragments that were visible at the core surfaces of VC35 and VC36 were picked from the sediment and rinsed with water. In addition, six sediment samples (65–135 g of sediment) were wet-sieved on a 1-mm-mesh sediment sieve, picked, identified and counted. Sample depths are noted in the Supporting Information. We used qualitative preservation characteristics of shells, including (lack of) abrasion, discoloration and bioerosion, and the preservation of fine surface details and periostracum, to distinguish autochtonous/parauthochtonous and transported (allochthonous) material (*sensu* Kidwell, 1986). The autochtonous/parauthochtonous material, resembling non- or limited-transported material, will further be referred to as *in situ* material. Only these *in situ* mollusc assemblages were used to define habitat characteristics following Meijer et al. (2021).

Pollen-based climate reconstructions

To quantitatively reconstruct past climate changes based on pollen data, transfer functions were applied to the pollen data from site VC35 (Waajen et al., 2024, available on the Neotoma palaeoecology database under DOI: 10.21233/E46K-G185, sample depths are noted in the Supporting Information.). The three pollen samples from the SD unit must be treated with caution because of low pollen counts. The pollen sample at 280 cm was almost barren and thus has not been included in this reconstruction. To infer modern climate–pollen relationships, pollen counts and climate variables were used from surface sediment samples across a wide variety of climate zones in Eurasia, extracted from the Eurasian Modern Pollen Database (EMPD2; Davis et al., 2020), containing 4350 reference samples (excluding samples with low counts). Canonical correspondence analysis (CCA) was applied in PAST software v.4.15 (Hammer et al., 2001) to select the climatic parameters with the largest explanatory power. Annual temperature (T_{ann}) and summer precipitation (P_{JJA}) were the parameters with highest eigenvalues, and were therefore used for climate reconstructions. To obtain a pollen–climate relationship, weighted-averaging partial least squares regression (WA-PLS; e.g. Birks, 2003; Chevalier et al., 2020) was used, which is a widely used regression technique to reconstruct precipitation and temperature, and accounts for the non-linear relationship of plant species and the environment (Chevalier et al., 2020). WA-PLS was applied with bootstrap cross-validated prediction errors and including a square-root species transformation using the program C2 v.1.8 (Juggins, 2007). Both T_{ann} and P_{JJA} were reconstructed from the pollen data of VC35 using WA-PLS (see model performance in Table 2). In addition, to identify locations of the closest analogues, the modern analogue technique (MAT) was applied in C2 v.1.8 with a squared chord distance. MAT is based on the degree of similarity between modern and fossil pollen assemblages (Chevalier et al., 2020 and references therein).

Lipid biomarker analysis

Lipid biomarkers were analysed in 26 samples taken from core VC35 (sample depths are noted in the Supporting Information). These samples were retrieved from the same depths as the pollen samples in Waajen et al. (2024), i.e. at intervals of 12 cm, adding two sediment samples from the Holocene sand unit at the top of the core for reference. For each sample, lipid biomarkers were extracted from 6–10 g of freeze-dried and homogenized sediments with dichloromethane (DCM)/methanol (MeOH) (9:1, v/v) using a Milestone Microwave Extractor Ethos-X, and subsequently separated into apolar, neutral and polar fractions over an activated Alox column using hexane/DCM (9:1, v/v), hexane/DCM (1:1, v/v) and DCM/MeOH (1:1, v/v) as eluents, respectively.

Long-chain n-alkanes

The apolar fractions, containing *n*-alkanes, were analysed on a Hewlett Packard HP6890 series gas chromatograph (GC) system coupled to a flame ionization/flame photometric detector (FID/FPD). Separation was achieved over a CP-Sil 5 fused silica capillary column (30 m, 0.32 mm, film thickness 0.10 µm) and a precolumn. The fractions were injected on column at 70°C, heating for 3 min to 130°C, subsequently to 320°C at 4°C min^{-1}, and then held isothermal at 320°C for 20 min. Long-chain odd-numbered *n*-alkanes with carbon chain lengths of 23 to 35 were identified on the basis of their retention time, and peak areas were integrated using Chemstation software.

Long-chain *n*-alkanes are produced by plants (Eglinton & Hamilton, 1967), and are generally resistant to degradation and well preserved in sedimentary archives, where they

Table 2. Performance for the pollen-climate WA-PLS models for summer precipitation (P_{JJA}) and annual temperature (T_{ANN}).

	P_{JJA} (mm per season)	T_{ann} (°C)
No. of components	4	4
RMSEP	56.388	2.437
R^2 bootstrap	0.7116	0.80499

© 2024 The Author(s). *Journal of Quaternary Science* Published by John Wiley & Sons Ltd.

represent an integrated vegetation signal of a larger area. Good preservation of higher plant-derived *n*-alkanes in sediments is indicated by carbon preference index (CPI) values > 1, reflecting the odd-over-even pattern that characterizes a terrestrial plant source (Bush & McInerney, 2013). The ratio of mid-chain ($C_{23} + C_{25}$) *n*-alkanes over the long-chain ($C_{29} + C_{31}$) *n*-alkanes, quantified in P_{aq}, can be used to differentiate contributions from vascular (long-chain) versus aquatic (mid-chain) plants (Ficken et al., 2000). The origin of the higher plant-derived *n*-alkanes can then be further specified on the assumption that woody vegetation synthesizes relatively shorter *n*-alkanes than non-woody vegetation, a difference that can be determined using the average chain length (ACL; Bush & McInerney, 2013).

Glycerol dialkyl glycerol tetraethers

The polar fractions contain both GDGTs and long-chain diols. First, GDGTs were analysed on an Agilent 1260 Infinity ultra-high-performance liquid chromatography (UHPLC) instrument, coupled to an Agilent 6130 single quadrupole mass detector with settings according to Hopmans et al. (2016), and separated by two silica Waters Acquity UPLC HEB Hilic (1.7 µm, 2.1 × 150 mm) columns, preceded by a guard column with the same packing. GDGTs were identified based on their $[M + H]^+$ ions in selected ion monitoring mode using Chemstation software B.04.02 and assuming a constant response for all GDGTs.

GDGTs are membrane lipids synthesized by marine archaea and (a) certain group(s) of bacteria, producing isoprenoid GDGTs (isoGDGTs; De Rosa & Gambacorta, 1988) and branched GDGTs (brGDGTs; Damsté et al., 2000), respectively. These compounds are at the base of several proxies used in palaeoclimate reconstructions. For example, the number of methylations attached to the alkyl chain of 5-methyl brGDGTs (MBT'_{5ME}; De Jonge et al., 2014), is empirically related to the mean air temperature for months above freezing (MAF), and can thus be used as a palaeothermometer (Weijers et al., 2007; Dearing Crampton-Flood et al., 2020). Additionally, the presumed soil-origin of brGDGTs is used in the ratio between brGDGTs and crenarchaeol, an isoGDGT solely produced by marine *Nitrosophaerota* (Sinninghe Damsté et al., 2002), to determine the contribution of fluvially transported soil OM to marine sediments, quantified in the Branched and Isoprenoid Tetraether (BIT) index (Hopmans et al., 2004). However, previous research has shown that brGDGTs can also be produced in coastal environments, potentially overprinting their initial soil-derived distribution, i.e. their temperature signal (Dearing Crampton-Flood et al., 2018; Peterse et al., 2009; Sinninghe Damsté, 2016).

Fortunately, the contribution of marine brGDGTs can be recognized using the weighted number of cyclizations in tetramethylated brGDGTs, captured in the parameter $\#rings_{tetra}$, where values > 0.7 indicate a primarily marine source of the brGDGTs (Sinninghe Damsté, 2016). Dearing Crampton-Flood et al. (2018) proposed that a marine contribution can be removed from the terrestrial temperature record by making use of the fact that marine *in situ* produced brGDGTs are also related to temperature, albeit bottom water temperature (BWT). We determine the relative contributions of soil and marine brGDGTs based on $\#rings_{tetra}$ assuming end-member values of 0.93 for a purely marine origin and $\#rings_{tetra}$ for samples with the highest BIT index values in our record as a soil end-member, following Dearing Crampton-Flood et al. (2018). The brGDGT distributions in VC35 suggest that parts of the record indeed contain some marine-produced brGDGTs, for which we correct the MBT'_{5ME} record using a BWT for the end of MIS 5a of 8.5°C to determine the marine MBT'_{5ME} (Boyer et al., 2013; Dearing Crampton-Flood et al., 2018). This BWT is based on the assumption that the difference between mean annual air temperature and BWT was similar to today, and that NW Europe was ~3°C colder during the end of MIS 5a than today, when BWT of the North Sea is 11.5°C (Guiot et al., 1989). A sensitivity test using 2°C lower or higher BWT results in reconstructed temperature offsets <0.5°C from those presented here. Subtracting the marine MBT'_{5ME} from the 'mixed' MBT'_{5ME} record results in a corrected MBT'_{5ME} record that represents the terrestrial temperature trend and can be translated into the average air temperature for MAF using the $BayMBT_0$ calibration model (Dearing Crampton-Flood et al., 2020).

Long chain diols

After GDGT analysis, the polar fractions were silylated by adding 10 µL, N,O-Bis(trimethylsilyl)trifluoroacetamide (BSTFA) and 10 µL pyridine per 0.5 mg of sample, and then heated at 60°C for 20 min prior to analysis for long-chain diols on an Agilent Technologies 7890B GC system coupled to an Agilent 5977B MSD using the same temperature programme as used for alkane analysis. The GC-MS device was equipped with a CP Sil-5 fused silica capillary column (25 m × 0.32 mm, 0.12 µm film thickness) using a constant helium flow rate. Targeted long-chain diols were identified and quantified from the total ion current (TIC) chromatogram on the basis of their characteristic mass fragments.

Long-chain diols are commonly detected in marine sediments, where the C_{28} and C_{30} 1,13-diol and 1,14-diol, and the C_{30} 1,15-diol are attributed to marine phytoplankton production (Rampen et al., 2007; Volkman et al., 1992). In contrast, the C_{32} 1,15-diol is tentatively assigned to freshwater algae (Lattaud et al., 2017b; Volkman et al., 1992). As such, its abundance relative to that of marine diols in coastal marine sediments ($\%C_{32}$ 1,15-diol) can therefore be used to reconstruct fluvial input in shelf seas (Lattaud et al., 2017a; Lattaud et al., 2017b).

Results

Diatoms

Diatoms are abundant and diverse in the BB clay unit, with *Delphineis surirella* and *Paralia sulcata* as most prominent species (Fig. 3). Diatom taxa have been organized into eco-groups representing lifeform and habitats along a salinity gradient. The majority of diatoms encountered thrive in marine and marine–brackish environments, with salinity >18‰. Marine–brackish diatoms are most abundant between 245 and 125 cm core depth, and there is an increase of marine taxa (salinity >30‰) towards the top of the clay unit. Brackish and freshwater taxa (salinity <9‰) are present in each sample in low quantities. This mixed assemblage of marine, brackish and freshwater taxa represents a shallow-marine environment with freshwater input. Most encountered diatom species are tychoplanktonic. Epiphytic taxa are present only in low quantities, and absent in some samples, indicating that submerged plants hosting these epiphytes were only sparsely present during deposition.

Molluscs

Mollusc shells from cores VC35 and VC36 and the preservation characteristics of these shells are presented as a composite in Fig. 4. The composite is based on the similar sedimentological succession of the two cores, and therefore samples are plotted

© 2024 The Author(s). *Journal of Quaternary Science* Published by John Wiley & Sons Ltd.

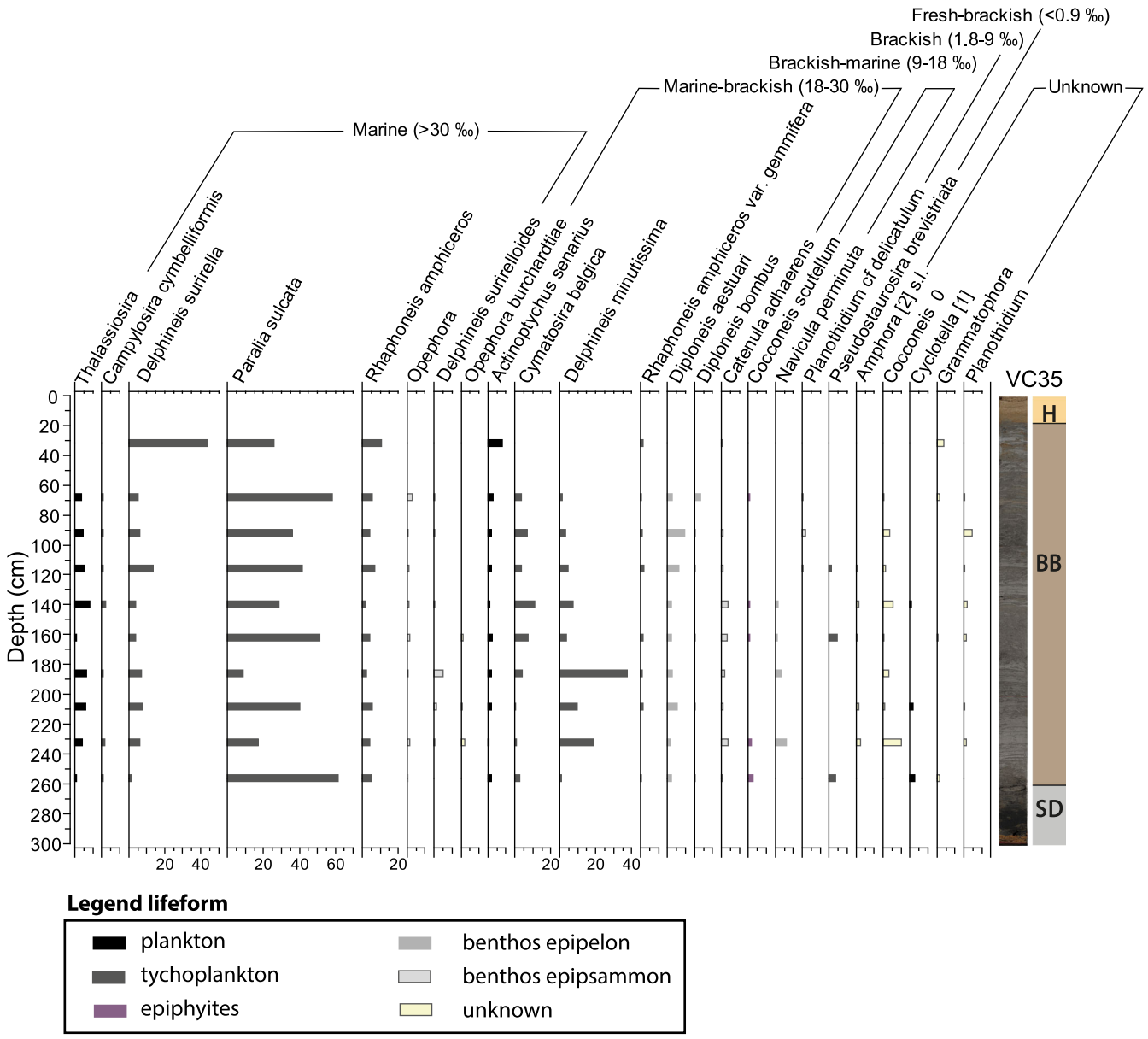

Figure 3. Percentage diagram of the most abundant diatom taxa (present in at least three samples and maximum abundance of at least 2%). Diatom taxa have been organized into eco-groups along a salinity gradient, and colours represent different lifeforms. The total count data can be retrieved from the Neotoma Palaeoecology database under DOI: 10.21233/CMDQ-BX08. [Color figure can be viewed at wileyonlinelibrary.com]

against the core depth where they were found. The composite log of VC35 and VC36 indicates to which sedimentary unit the molluscs belong. Shell numbers are low, so interpretations are somewhat tentative. All shells and fragments sampled from the SD unit are considered allochthonous. The level of abrasion indicates high-energy conditions before or during deposition of the SD unit, but offers no insights into the exact palaeoenvironment. Shells and fragments taken from the BB clay unit show mixed preservation characteristics with both allochthonous and *in situ* components. A strongly worn component is mixed with specimens characterized by very fine surface details and well-preserved periostracums, as well as a single paired *Macoma balthica* specimen (Fig. 4b-2). All *in situ* (or autochthonous) taxa (in orange in Fig. 4–2a) combined represent a low-energy marine setting with water depths around or below the storm-wave base (generally 15–40 m water depth). Notable is the *in situ* occurrence of the high-boreal to arctic *Macoma calcarea* (Fig. 4b-3). Within the BB clay unit, at around 43 cm (VC35) and 45 cm core depth (VC36), a 3-cm-thick shell-rich layer was found with a matrix consisting of coarse sand and gravel-sized flint (with pebbles up to 3 cm in size). This layer contains reworked and mixed mollusc shells, including one of Middle or Early Pleistocene age (*Macoma obliqua*, Fig. 4b-1), indicating (fluvial or transgressive) reworked faunas.

Pollen-based climate reconstruction

WA-PLS-based reconstructions for both summer precipitation (P_{JJA}) and annual temperature (T_{ann}) show some fluctuations, but no long-term trends (Fig. 5). The two sample points from the SD unit have low pollen abundances (50–60 counts per sample), with a barren sample in between, providing a more tentative climate signal compared to the samples from the BB clay unit. P_{JJA} averaged 240 (±56) mm, with fluctuations of up to 52 mm. T_{ann} has an average of 6°C (±2.4), with fluctuations of up to 3°C, where the largest shift occurs between the lowest two samples. The EMPD used contains good analogues for the fossil samples, as all fossil samples have dissimilarity values to their closest modern analogue within the 5th percentile, where most samples fall within the 2nd percentile dissimilarities, based on MAT (Fig. 5). The three closest modern analogues per pollen sample from VC35, determined by MAT, are mainly

© 2024 The Author(s). *Journal of Quaternary Science* Published by John Wiley & Sons Ltd.

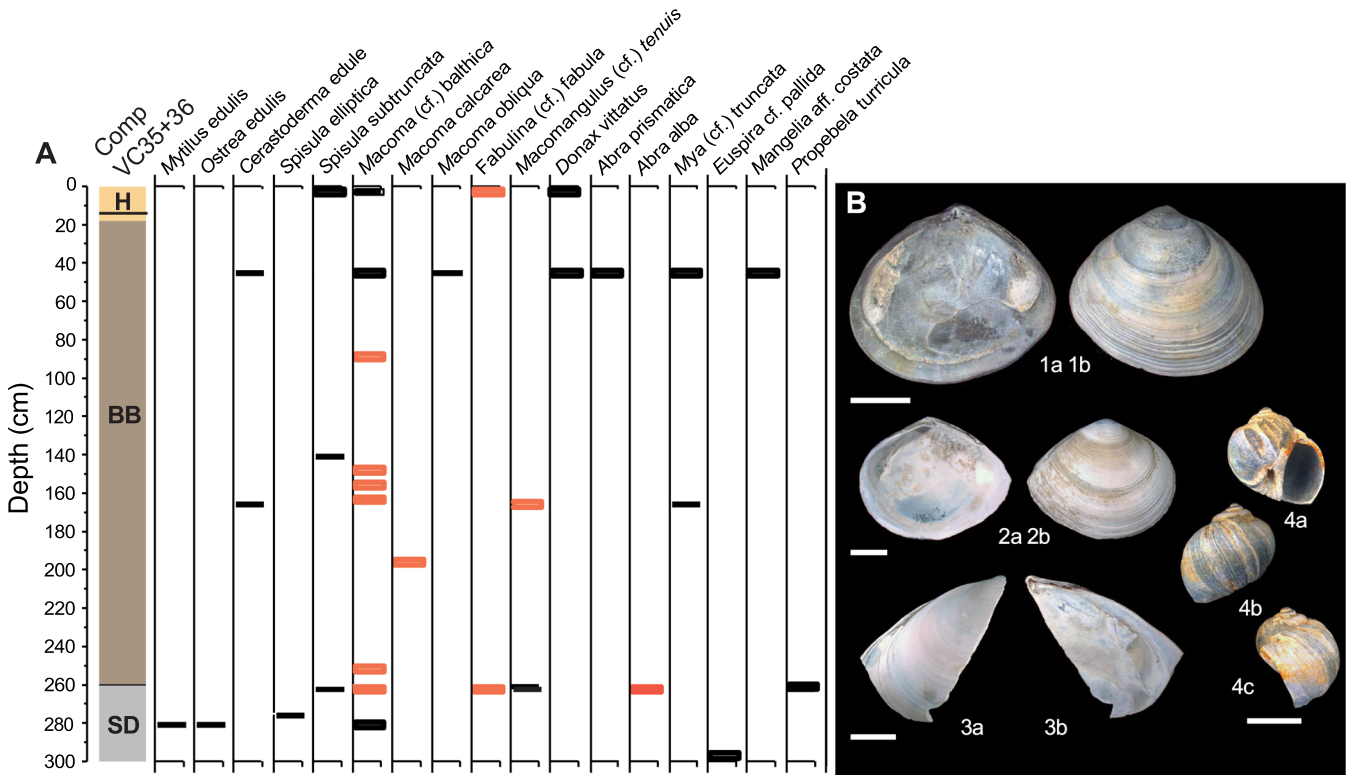

Figure 4. (A) Mollusc occurrences, composite of VC35 and VC36. Orange bars represent very well-preserved specimens, probably representing *in situ* occurrences, and black bars represent worn, allochthonous (transported) specimens. (B). Scale bars 5 mm. 1a,b. *Macoma obliqua* (Sowerby, 1817). VC35, 43 cm core depth; worn specimen, reworked from Middle or Early Pleistocene deposits (RGM.1365332). 2a,b. *Macoma balthica* (Linnaeus, 1758). VC35, 161 cm core depth; specimen with very fine surface details and periostracum indicating lack of transport (RGM.1365333). 3a,b. *Macoma calcarea* (Gmelin, 1791). VC36, 195 cm core depth; sharp-edged fragment with very fine surface details and periostracum, indicating lack of transport, arctic to subarctic species (RGM.1365334). 4a,b. *Euspira* cf. *pallida* (Broderip & Sowerby, 1829). VC35-3, 296 cm core depth; worn specimen, cold boreal to subarctic species (RGM.1365335). [Color figure can be viewed at wileyonlinelibrary.com]

clustered around the Baltic Sea, including the Baltic states and southern to middle Scandinavia (Fig. 6).

Biomarkers

Long-chain n-alkanes

Plant wax *n*-alkanes were present in all samples in concentrations varying between 12 and 96 μg g^{-1} OM (based on LOI, Waajen et al., 2024). The lowest concentrations are in both sand units. Higher concentrations occur in the BB clay unit and reach a maximum value at 140 cm core depth. The *n*-alkanes have CPI values > 1 in all samples (Fig. 7), indicating good preservation. Thus, these biomarkers can be used to provide information on the vegetation composition in the nearby drainage basin during deposition.

The *n*-alkane distribution clearly differs between the three sedimentary units (Fig. 7). The P_{aq} values, which differentiate submerged, emergent (able to endure inundation) and fully terrestrial vegetation (Ficken et al., 2000), arer on average 0.47 in the SD unit, indicating a mixed contribution of emergent and submerged plants; 0.32 in the BB clay, indicating a relatively larger contribution from emergent and terrestrial vegetation; and 0.55 in the Holocene sand unit, indicating *n*-alkanes mainly derived from submerged taxa. $ACL_{27\text{-}33}$ indicates that relatively more *n*-alkanes from non-woody species are represented in the lower part of the core (below 250 cm, corresponding to the SD unit and the lowest part of the BB clay unit), and that relative contributions of woody vegetation abruptly increase above 250 cm. There is no clear difference in ACL between the Holocene and BB interval, suggesting a similar ratio of plant waxes from woody versus non-woody vegetation was transported to this site during both depositional phases.

Glycerol dialkyl glycerol tetraethers

GDGTs are present in all samples, with brGDGT concentrations varying from 84 to 4899 μg g^{-1} OM. The BIT index in the SD unit has values around 0.6, indicating mixed marine- and terrestrially sourced OM. In the BB clay unit, BIT index values are close to 0.9 (Fig. 7), which indicates that most of the OM in this interval has a terrestrial origin. This contrasts with the OM in the Holocene sand unit, where a BIT index value around 0.15 indicates that most of the OM is marine in origin. The parameter $\#rings_{tetra}$ (Fig. 7) is close to 0.3 in the SD unit and in the BB clay units. In the Holocene sand unit and the top two samples of the BB clay unit $\#rings_{tetra}$ values range from 0.45 to 0.85, indicating larger contributions of *in situ* marine-produced brGDGTs. Assuming a linear relation in the mixing of marine- and terrestrially sourced brGDGTs, we find that the SD unit contains on average 14% of marine-produced brGDGTs, the BB clay unit 7% and the Holocene sand unit 77%. This implies that the temperature signal of the soil-derived brGDGTs is hardly affected in the BB clay unit but is marked by marine overprints in the sandy sections of the record.

Owing to the low percentages of marine-produced brGDGTs in the SD and BB clay units, only small corrections were applied to the soil-derived temperature signal (see 'Lipid biomarker analysis' in the Methods). MAF during deposition of the SD unit was on average 9.4°C, followed by a drop in temperature at the start of deposition of the BB clay unit, where MAF was 7.7°C on average. The highest reconstructed

© 2024 The Author(s). *Journal of Quaternary Science* Published by John Wiley & Sons Ltd.

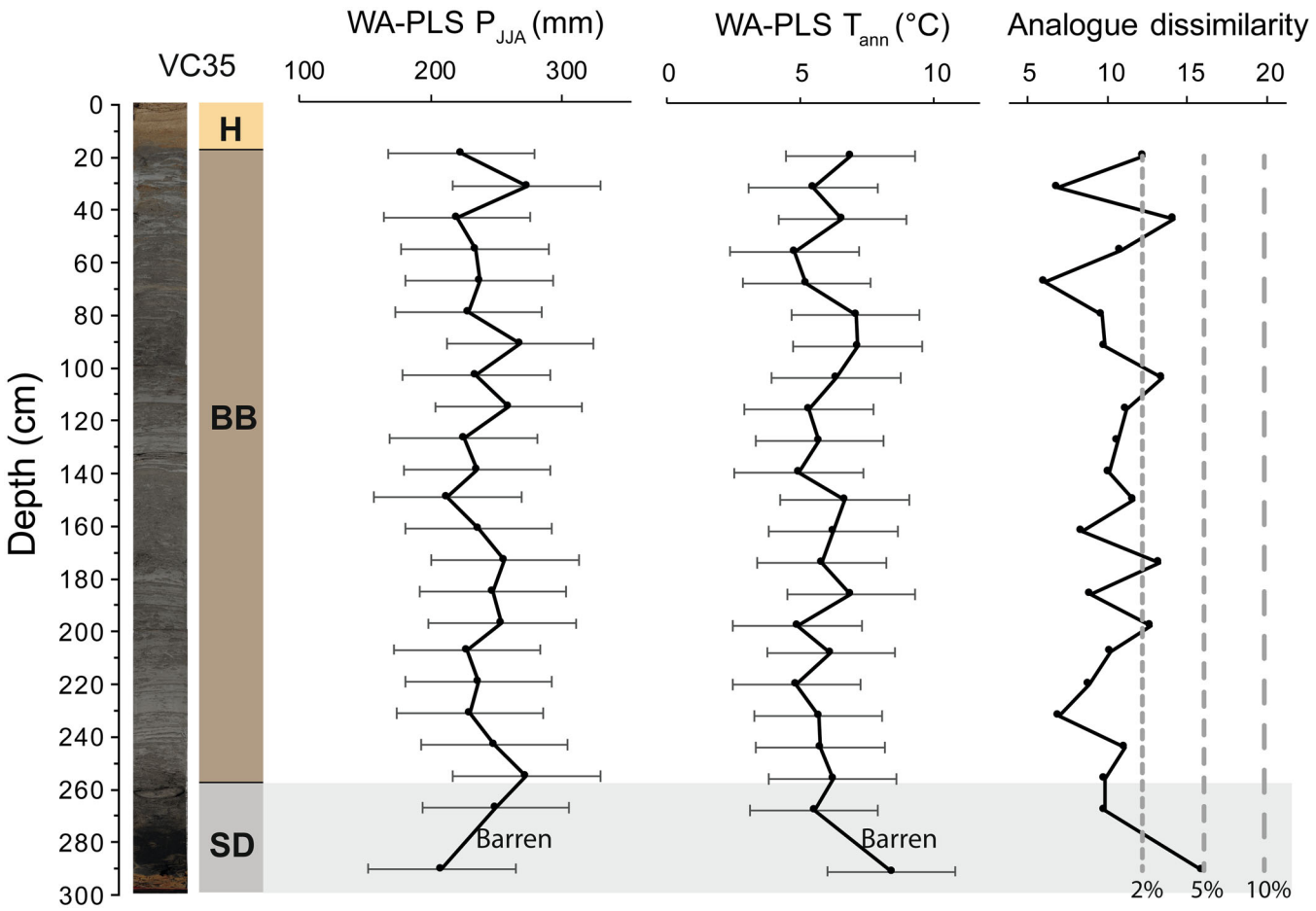

Figure 5. Summer precipitation (P_{JJA}) and annual temperature (T_{ann}) reconstructions of VC35 based on WA-PLS regression. Unit SD is shaded as these samples contain lower pollen counts and reconstructions are therefore more uncertain. The error bars represent the sample-specific estimated standard errors of prediction (eSEPs). The analogue dissimilarity is based on the Modern Analogue Technique and represents the distance to the modern analogues and fossil data. The dashed lines indicate the 2nd, 5th and 10th percentiles of all squared chord distances in the calibration dataset. [Color figure can be viewed at wileyonlinelibrary.com]

temperature within the BB clay unit is 9.2°C at a depth of 150 cm down core. This sample is derived from the sandiest interval of the BB clay unit, fitting with the general pattern of sandy intervals deposited under slightly warmer conditions than clay-rich intervals. There is a cooling trend from 80 cm core depth towards the top of the BB clay unit (18 cm core depth), with MAF reaching 5.6°C.

The relatively high amount of marine-produced brGDGTs in the Holocene marine sediments hampers accurate soil-derived reconstruction of air temperature. Instead, the BWT for the Holocene is reconstructed using the marine calibration of Dearing Crampton-Flood et al. (2018). Currently, the temperature for MAF equals mean annual air temperature, as monthly averaged winter temperatures are above freezing. As current air temperature is ca. 1°C lower than North Sea BWT, subtracting 1°C from the reconstructed Holocene BWT provides an indication for MAF, resulting in an average temperature of 11.9°C (Fig. 7). Compared to the MAF of the Holocene, the MAF during deposition of the SD unit was ca. 2.5°C lower, and the MAF during deposition of the BB clay unit was on average 4.2 °C lower.

Long-chain diols

The parameter $\%C_{32}$ 1,15-diol varies between 15% and 31% within the core, with an average value of 25 ± 5% in the SD unit ($n = 2$), 23 ± 3.5% in the BB clay unit ($n = 22$) and 31 ± 1.6% in the Holocene sand unit ($n = 2$) (±1σ). In all units, the C_{30} 1,15-diol is the most abundant.

Discussion

Depositional environment

Both unit SD and the Holocene sand unit represent high-energy sea floor depositional environments judging from the grain size and seismic reflection configuration. However, the two units were deposited in different marine environments. The low terrestrial input (BIT index values around 0.1) in the Holocene unit resembles the present-day, open marine environment. In addition, the *n*-alkanes in the Holocene sand are mainly derived from submerged and floating, aquatic vegetation. On the other hand, the SD unit is characterized by a relatively high contribution of terrestrially sourced organic material (higher BIT index values, around 0.6), where most *n*-alkanes are derived from coastal wetlands holding emergent vegetation. We interpret unit SD as representing a marine environment affected by river discharge, which is also supported by the relatively high abundance of $\%C_{32}$ 1,15-diol. Compared to the modern situation, more soil material was transported to this site during deposition of unit SD. From this, we infer that the coast was closer to the study site compared to the modern situation, as a result of the seaward movement of the shoreline in response to relative sea-level lowering.

© 2024 The Author(s). *Journal of Quaternary Science* Published by John Wiley & Sons Ltd.

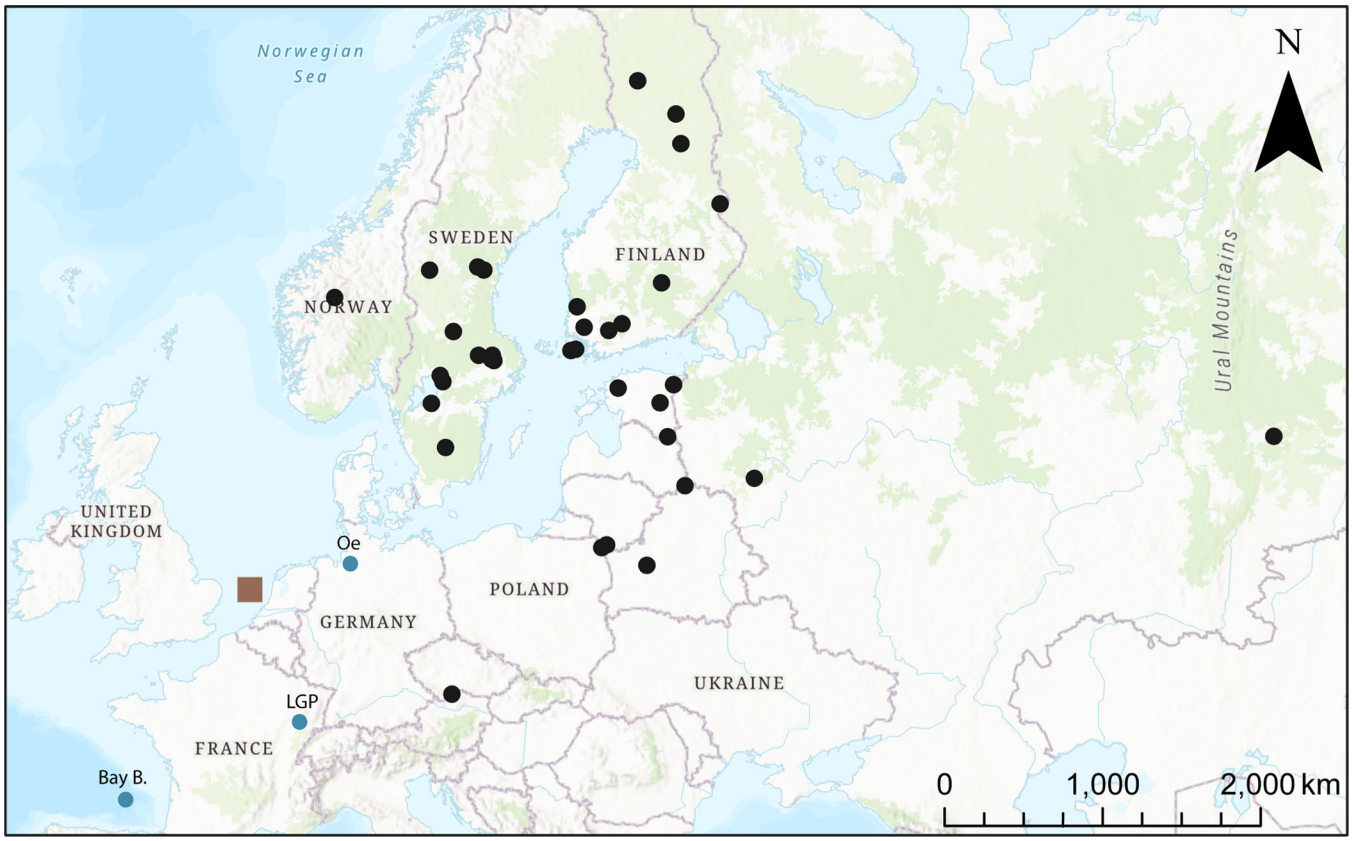

Figure 6. Map indicating the three closest modern analogues from the Eurasian Modern Pollen Database (EMPD2) per VC35 pollen sample (black dots). The location of VC35 is indicated by the brown square. Locations of key sites Oerel (Oe), La Grande Pile (LGP) and Bay of Biscay (Bay B.) are indicated in blue. [Color figure can be viewed at wileyonlinelibrary.com]

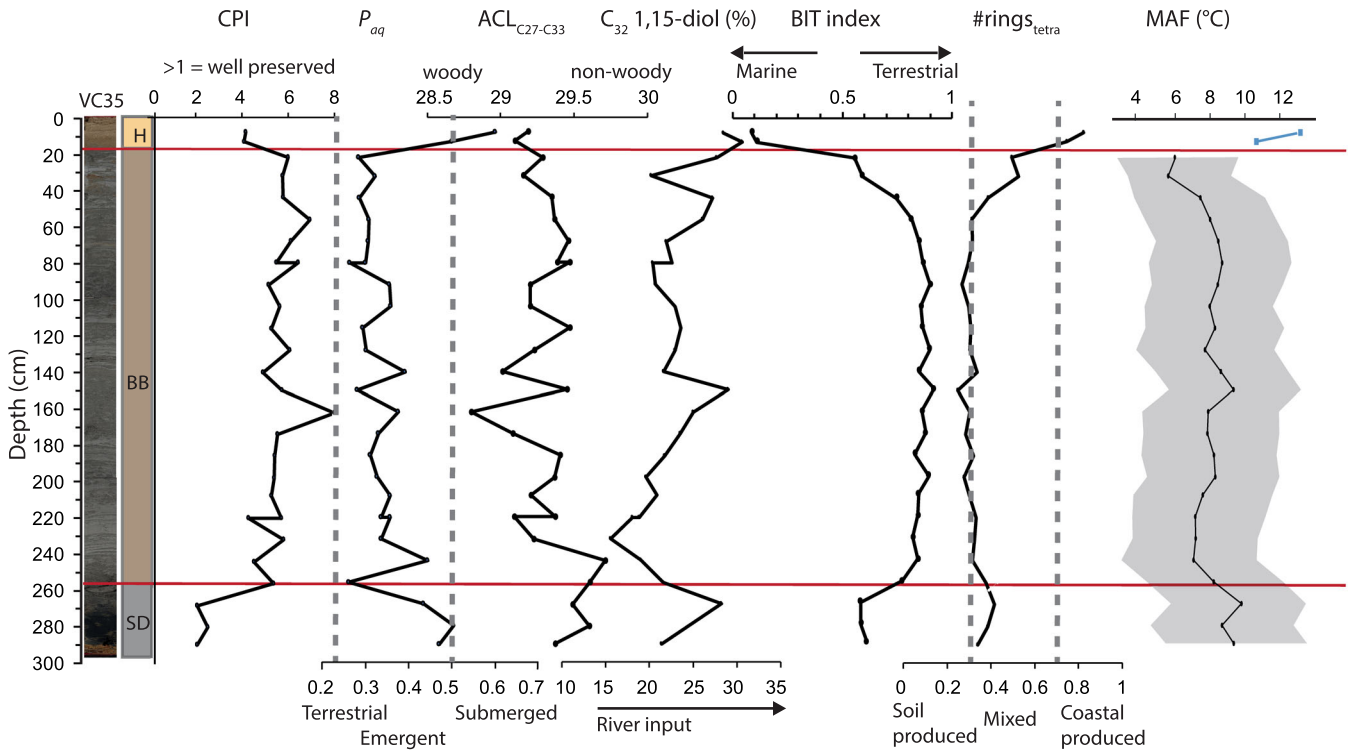

Figure 7. Lipid biomarker proxies for core VC35, where the red horizontal lines indicate the sedimentary unit boundaries. Alkane proxies: CPI (carbon preference index) indicating good preservation of OM; P_{aq} indicating contributions from higher plants versus aquatic vegetation; ACL (average chain length) indicating woody versus non-woody vegetation. $\%C_{32}$ 1,15-diol indicates river input. GDGT proxies: BIT (branched and isoprenoid tetraether) index indicating terrestrial OM input; $\#rings_{tetra}$ indicating the soil versus marine source(s) of brGDGTs; and brGDGT based temperature for the months above freezing (MAF), with the 1σ error (4°C on average) indicated by the grey envelope. The blue line represents MAFs for the Holocene sand unit and are based on BWT, as explained in 'Biomarkers' in the Results. [Color figure can be viewed at wileyonlinelibrary.com]

© 2024 The Author(s). *Journal of Quaternary Science* Published by John Wiley & Sons Ltd.

The BB clay unit was deposited in a shallow, restricted marine setting, different from the more open marine conditions represented by the underlying and overlying sand units. Although multiple studies of the BB Fm (e.g. Oele 1971; Zagwijn, 1983) described a brackish or freshwater (lacustrine) environment for much of the unit, there is abundant evidence for a marine depositional environment, including the presence of *in situ* marine molluscs (Fig. 4), marine (tycho)planktonic diatom assemblages (Fig. 8d, e), dinoflagellate cysts and sporadic organic linings of foraminifera (Waajen et al., 2024). Our interpretation of a shallow-marine setting is supported by foraminifera and ostracod data from core VC34 (Forthcoming Europe's Lost Frontiers, Volume 3: Environment). The *in situ* mollusc component represents a low-energy, shallow-marine environment around or below storm-wave base, which is confirmed by the diatom data. Although the exact water depth during deposition is difficult to constrain, we suggest that it was shallower than present water depth (39 m), and is estimated to have been between ca. 10 and 35 m. This is based on the depth of the storm-wave base around the modern Dutch coast, which is generally around 13–20 m water depth (Cleveringa, 2000; Van der Valk, 1992; Van der Werf et al., 2017). Lower sea level and a corresponding smaller basin during deposition of the BB clay unit will have limited the fetch of storm waves, reducing their wavelengths (e.g. Le Roux, 2009) and therefore the depth of the storm-wave base.

Our study site received a high input of terrestrial OM during deposition of the BB clay unit. The high input of terrestrial OM is reflected in high BIT index values, abundance of pollen, biomarkers of vascular plants, and elemental indicators of terrestrial input [log(Al/Ca) and log(Ti/Ca)] (Waajen et al., 2024; Fig. 8f, g). The $\%C_{32}$ 1,15-diol values that are continuously above 15% throughout the record provide evidence that site FG was influenced by fluvial input during deposition of all sedimentary units (Lattaud et al., 2017a). Input of soil material was higher during the deposition of the BB clay unit than during accumulation of the sands above and below, indicating enhanced soil erosion on land during deposition of the BB clay unit. The clear combination of terrestrial and marine influences suggests a pro-deltaic or outer-estuarine depositional environment close to the coast.

The upper 50 cm of the BB clay unit suggests a change towards a more open marine depositional environment, indicated by a simultaneous decrease in terrestrial input (lower BIT index values and relatively low Ti/Ca and Al/Ca ratios) and a relative increase in fully marine diatom taxa (salinity >30‰). This trend is not caused by bioturbation of the overlying Holocene marine sediments, as the *n*-alkane proxies show an abrupt transition from the BB clay unit into the Holocene sediments, related to the hiatus at the top of the BB clay unit (Fig. 7). This interval in both cores VC35 and VC36 contains the coarse-grained, poorly sorted, shell-rich layer with pebbles (see 'Molluscs' in the Results) indicative of higher-energy conditions. More open marine conditions could have resulted from either a relative sea-level rise, or a decrease in terrestrial input. The former is less plausible as deposition occurred during a falling stage of eustatic sea level (Fig. 8a). Our findings of an increasingly open marine environment towards the top of the BB clay unit seem to contradict earlier studies of Zagwijn (1983). He concluded that marine conditions were limited to the earliest phase of deposition, followed by a freshening upwards towards a freshwater (lacustrine) environment. Regarding the hiatus between the Brown Bank clay unit and Holocene deposits, it is likely that the top of the BB Fm has been eroded in this location, and potentially deposits of a subsequent freshwater environment have not been preserved at this site.

The sediment, as well as the pollen and terrestrial lipid biomarkers, were transported from terrestrial setting(s) into the adjacent marine environment. The position of the BB Fm, just west of the reconstructed Rhine channel belt active

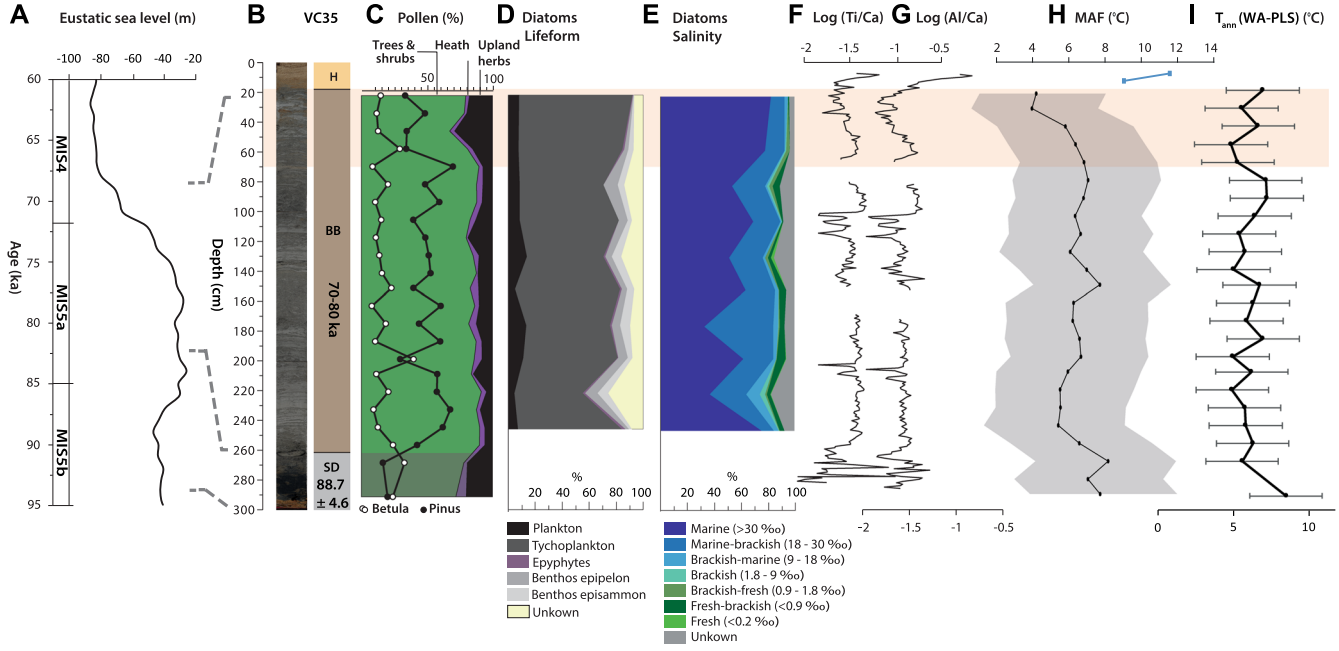

Figure 8. Comparison of eustatic sea level to data from VC35, where the top 50 cm of the clay unit, which is referred to in 'Depositional environment', is highlighted in orange. (A) Eustatic sea-level curve (Spratt & Lisiecki, 2016); (B) core photo and simplified core log of VC35, including unit names and age ranges based on OSL dating (Waajen et al., 2024); (C) summary of the pollen diagram in percentages of VC35 (Waajen et al., 2024); (D) diatom assemblages in percentages grouped under lifeform; (E) diatom assemblages in percentages grouped under preferential salinity regimes; (F) logarithmic ratio between titanium and calcium based on XRF data (Waajen et al., 2024); (G) logarithmic ratio between aluminium and calcium based on XRF data (Waajen et al., 2024); (H) reconstructed air temperature for months above freezing (MAF) based on brGDGTs; (I) reconstructed mean annual air temperature based on WA-PLS of the pollen assemblages. [Color figure can be viewed at wileyonlinelibrary.com]

© 2024 The Author(s). *Journal of Quaternary Science* Published by John Wiley & Sons Ltd.

during MIS 5 and 4 (Busschers et al., 2007; Hijma et al., 2012; Peeters et al., 2015), makes a Rhine–Meuse sediment source for the BB clays the most plausible. However, smaller contributions from other fluvial systems cannot be excluded. A glacial sediment source is not expected, as the pollen assemblages contain very limited amounts of reworked Tertiary pollen. In contrast, the marine diatoms and molluscs represent the local marine environment and therefore have more local implications.

Terrestrial vegetation

The abundance of preserved terrestrial OM within the BB Fm provides a unique opportunity to reconstruct the regional terrestrial landscape that has been lost by erosion elsewhere. There may be a time lag between the production of terrestrial OM, mobilization and deposition offshore, as the terrestrial biomarkers and pollen were probably produced in the period prior to increased soil erosion, and thus mainly represent vegetation of the time period before deposition. The vegetation signal resembles the last phase of the Odderade interstadial (Waajen et al., 2024), time equivalent to the first half of MIS 5a, while deposition in the marine environment probably occurred around the last part of MIS 5, representing the MIS 5–4 transition. At the transition from unit SD to BB clay, we observe a relative increase of *n*-alkanes derived from higher plant material at the cost of those from submerged and emergent vegetation (wetland and aquatic). ACL shows relatively more *n*-alkanes derived from non-woody vegetation, such as grasses, in the SD unit while relatively more *n*-alkanes derived from woody vegetation are present in the rest of the record (Fig. 7). The pollen assemblages provide a similar perspective on the vegetation. Analyses of samples from the SD unit are less reliable than those from the BB clay unit, owing to low pollen counts (50–60 counts per sample) as the result of low pollen concentrations (only 330–425 pollen grains cm^{-3}, compared to concentration in the BB clay unit between 5500 and 48000 grains cm^{-3}). Despite the lower pollen counts in the SD unit, the pollen data indeed indicate a more open landscape, with a higher concentration of grasses (Poaceae and Cyperaceae) compared to the record of the BB clay unit. There, the pollen assemblage consists of ~80% tree and shrub pollen, dominated by *Pinus* and *Betula* (Fig. 8c). The pollen composition remains stable in the BB clay unit, up to 60 cm core depth, where an increase in grasses and a decrease in *Pinus* indicates the transition into a more open landscape compared to the rest of the BB clay unit. This transition is not observed in the *n*-alkane record.

Another pollen record from the BB Fm in this region shows a vegetation succession that differs from the one in our study site (Waajen et al., 2024). Core P5-4 (GSN number BP050004), only 17 km northeast from VC35 (Fig. 2; core 2 in fig. 2 in Zagwijn 1983; pollen data available at www.neotomadb.org), contains BB clay deposits with a stadial pollen assemblage, consisting of some 50% herbaceous pollen (Zagwijn, 1983). Sparsely present ostracods in the BB clay of P5-4 represent shallow-water euryhaline groups, and are interpreted as being reworked in a non-marine depositional environment (Du Saar, 1970). The BB clay at VC35 and P5-4 must have been deposited during different time intervals, in a different environment under different climate conditions (marine, interstadial at VC35; freshwater, stadial at P5-4). We can conclude that the BB Fm is a diverse deposit, with preservation of multiple depositional phases from different periods and substantial lateral variability over relative short distances.

Climate reconstruction

In general, both brGDGT- and pollen-based temperatures provide evidence of cooler conditions during the MIS 5–4 transition than at present (Fig. 8h, i). brGDGTs reflect that, on average, temperatures during deposition of the SD unit were ca. 2.5°C lower than the reconstructed Holocene temperatures. During deposition of the BB clay unit conditions were on average 4.2°C colder compared to our reconstructed Holocene temperatures. The reconstructed Holocene temperature of 11.9°C is similar to the current mean T_{ann} at buoy P11-B, a weather station in the North Sea (11.2°C; KNMI, 2024), and thus we can conclude that temperatures during deposition of the SD and BB clay units were lower than present. The pollen assemblages are typical for the end phase of an interstadial (Waajen et al., 2024), and reconstructed climate and modern analogues compare to modern conditions around the Baltic Sea (Fig. 6). Pollen-based reconstructed summer precipitation (P_{JJA}; 240 ± 56 mm) is similar to the modern summer precipitation in Den Haag (the closest city to the study site; 235 mm) and similar to the average for the Netherlands (226 mm; CCKP, 2024). This shows that differences in vegetation type and cover between the MIS 5–4 transition and the Holocene were mainly influenced by temperature and not by precipitation differences.

Pollen-based T_{ann} is slightly lower than MAF, indicating that winter temperatures must have been below 0°C. As both pollen and terrestrial biomarkers originate from land and are transported to the marine environment, we can assume a similar delay between production and deposition of both proxy materials. Both records suggest slightly warmer conditions during deposition of the SD unit than during deposition of the BB clay unit, despite the low pollen abundances in the SD unit. Both records in general indicate only small temperature variations (<2°C) within the BB clay. In the top part of the BB clay unit, pollen-based temperatures remain constant while the brGDGTs indicate a cooling. A possible explanation could be that changes in seasonality impacted the growing season of soil microbes differently than that of vegetation. Although the pollen assemblages do show an increase in herbs compared to trees, in line with dropping temperatures, the presence of some thermophilous taxa in the top sample (*Fagus*, *Quercus*) distort this signal. It is presently uncertain whether these thermophilous taxa are *in situ* or represent reworked (older) or bioturbated (younger) pollen. This general cooling towards the top of the BB clay unit is accompanied by an increase in marine diatom species (Fig. 8e) and a decrease of terrestrial input and may be linked to the transition into MIS 4.

The low air temperatures during deposition of the BB clay unit are in line with evidence of subarctic–arctic water conditions in the marine environment, represented by *in situ* *Macoma calcarea* at 200 cm core depth. These (sub)arctic marine conditions in the southern North Sea during the MIS 5–4 transition have not been described earlier. Although we do not have a sea-surface-temperature reconstruction for this site, the (sub)arctic marine water is in line with the low terrestrial air temperatures at this location. The relative decoupling of ocean water and air temperatures described for the Bay of Biscay (Sánchez Goñi et al., 2013) during the MIS 5–4 transition thus probably did not affect the shallow southern North Sea.

Other temperature records in Europe of MIS 5a do exist, but the transition into MIS 4 is rarely preserved. In the Bay of Biscay, ca. 1000 km southwest of our site, sea surface temperature reconstructions made for the MIS 5–4 transition

© 2024 The Author(s). *Journal of Quaternary Science* Published by John Wiley & Sons Ltd.

show two cycles of cooling and warming at the end of MIS 5a, before cold conditions of MIS 4 set in (Sánchez Goñi et al., 2013). We do observe minor warming of air temperatures within the central part of the BB clay unit (Fig. 7), but much smaller in magnitude than those for the open ocean. Two terrestrial western European sites with air-temperature reconstructions for late MIS 5a are Oerel (NW Germany), which had more continental climate conditions, and La Grande Pile (central France), which is located farther south (Fig. 6) and experienced a more temperate climate despite being more than 300 m above MSL. In Oerel, the end of the Odderade interstadial has a T_{max} (mean temperature of the warmest month of the year) of approximately 11–12°C and a T_{min} (mean temperature of the coldest month) of −10 to −13°C (Sejrup & Larsen, 1991). This temperature range is comparable to the T_{ann} and MAF temperature records of this study, but the early MIS 4 is missing in this record. In the record of La Grande Pile, Coleoptera-based temperatures remain high at the end of the Saint Germain II interstadial (linked to MIS 5a) with a T_{max} of 16–19°C and a T_{min} of 0–6°C (Ponel, 1995), reasonably in line with modern values of 18.5°C and −0.5°C respectively (Rousseau et al., 2007). In the La Grande Pile record, the transition from the temperate Saint Germain II interstadial (MIS 5a) into the pleniglacial (MIS 4) is very abrupt, with about 5°C cooling within 50 cm of sediment (Guiot et al., 1989). This terrestrial record (Woillard, 1978) contains the same cycles of cooling and warming as observed in the records from the Bay of Biscay (Sánchez Goñi et al., 2013). In comparison with these records, our record corresponds to only part of the MIS 5–4 transition. Although our record only represents a short window of past conditions, its high sedimentation rate (Waajen et al., 2024) captured the trends during the cooling phase in detail, as well as the response to this cooling in both the marine and terrestrial environments of the North Sea basin.

Implications for climate and sea level at the MIS 5–4 transition

Continued marine conditions around the MIS 5–4 transition have not been described earlier for the North Sea region. The evidence of a (sub)arctic marine environment uncovered by our work (Figs. 4 and 8) shows that most of the drop in sea level lagged climate cooling during this time period. Our results indicate that water depth during BB clay deposition was probably at least 10 m (see 'Depositional environment' above). As the seabed at our study site was ~33 m below modern MSL during deposition (Waajen et al., 2024), local sea level in the southern North Sea during the MIS 5–4 transition (70–80 ka; age of the BB clay unit at site FG) was probably less than 23 m below modern MSL. According to the reconstruction by Spratt & Lisiecki (2016), global sea level dropped deeper than −31 m below MSL after 78 ka and reached −65 m below MSL at 70 ka. The uncertainty of the OSL ages from the BB sediments limit exact comparison to the global sea-level curve, but it is clear that deposition occurred during a falling stage of global sea level. This was also used to explain the preservation of sediments from MIS 4 in an estuarine setting, farther to the east (Törnqvist et al., 2000). Global sea-level data for MIS 5a derived from corals display large scatter between sites (Medina-Elizalde, 2013), but generally suggest that sea level was higher than the eustatic sea-level curves of Lisiecki & Raymo (2005), Rohling et al. (2009) and Waelbroeck et al. (2002). In addition, new data from Indonesia also suggest relatively high global mean sea level, around −12 m, during MIS 5a (Weiss et al., 2022). Thus, a mismatch between eustatic sea-level models and sea-level index points for this time period is a general issue, and not site-specific. Most sea-level reconstructions are based on benthic $\delta^{18}O$ records, which relate to both sea level and temperature. Eustatic sea level could have lagged temperature at the MIS 5–4 transition, as observed for relative sea level in our study, remaining high for a longer period than most models simulate. The delay in sea-level drop compared to cooling might be explained by the time needed for the build-up of ice caps, which generally occurs well after atmospheric cooling starts.

The major difference between the position of our sea-level indicators and predicted global mean sea level at the time of deposition (latest MIS 5a – earliest MIS 4) remains enigmatic. Glacio-isostatic effects, i.e. suppression during deposition followed by uplift during and after deglaciation, would require an ice sheet much larger than present during MIS 2, as for the latter period the study area is predicted to have been situated on the southern side of the fore bulge (Busschers et al., 2007; Kiden et al., 2002). Current estimates on MIS 4 ice extent suggest the BIIS and FIS in the North Sea area were smaller compared to the maximum ice extent of the LGM (Batchelor et al., 2019; Dalton et al., 2022; Toucanne et al., 2023), although uncertainties on the size, shape and timing of growth of the BIIS and FIS during MIS 4 remain.

The BB Fm represents a sink for terrestrial OM that has not been preserved onshore, and therefore contains new information from a period generally missing from onshore records. In the terrestrial environment, the end of MIS 5a has only been found in specific settings protected from erosive processes during the subsequent glacial period, usually depressions such as lake beds or peat bogs [e.g. the Eifel maar lakes (Riechelmann et al., 2023), La Grande Pile (Guiot et al., 1989)]. The lag between sea-level and temperature trajectories that we observe created a sediment preservation window during the onset of the last glacial period in a shallow marine environment. The BB Fm not only gives us insights into the cold marine environment that persisted, but also information on terrestrial landscapes lost to erosion. Using a combination of terrestrial proxies and marine indicators, we can now pinpoint the cooling of the MIS 5–4 transition, see the change from an open marine to pro-deltaic environment, and reconstruct how the stable, late interstadial vegetation is replaced by more herbaceous vegetation. More complete sections of the BB Fm are visible on new seismic profiles from the area around the Brown Bank ridge. They show evidence of multiple depositional phases, which will provide a more complete understanding of this unique record of climate, sea-level and environmental change.

Conclusions

A multi-proxy analysis of vibrocores from the southern North Sea provides new and detailed insights into the changing climate, regional sea level and palaeoenvironment during the transition of MIS 5a to MIS 4. Within the BB Fm, the transition from the sand dune unit into the BB clay unit resembles the transition from an open marine to a restricted marine environment, relatively close to deltaic or estuarine lowland that provided terrestrial sediment and organic matter. This change within the marine environment is forced by the climate deterioration during the MIS 5–4 transition. Evidence of cold marine conditions indicates that sea-level fall was lagging temperature, creating an offshore preservation window for terrestrial sediments that have typically been eroded on land. Towards the top of the BB unit a cooling is reconstructed, which is simultaneous to a decrease in terrestrial input, and can be related to the start of MIS 4. The wide extent and varying thickness of the BB Fm presents a unique opportunity to analyse one of the key transitions in Pleistocene climate history.

© 2024 The Author(s). *Journal of Quaternary Science* Published by John Wiley & Sons Ltd.

Acknowledgements. We thank Geurt Verweij from Waardenburg Ecology for providing the diatom analyses and helping with the interpretations. In addition, we thank the 'Europe's Lost Frontiers' project of the Department of Archaeological and Forensic Sciences, University of Bradford (UK), funded by a European Research Council Advanced Grant, for sharing unpublished foraminifera and ostracod results. Finally, we would like to acknowledge the guidance and assistance of Klaas Nierop, Desmond Eefting, Mariska Hoorweg, Antoinette Dikkenberg and Sunning Hou during the lipid biomarker analyses. The research was funded by TNO – Geological Survey of the Netherlands.

Data availability statement

The biomarker data is provided as supplementary file to this paper. All other data that support the findings of this study are openly available in the Neotoma Paleoecology Database at https://neotomadb.org.

Supporting information

Additional supporting information can be found in the online version of this article.

Abbreviations. ACL, average chain length; BB, Fm Brown Bank Formation; BIT, index Branched and Isoprenoid Tetraether index; CPI, Carbon Preference Index; GDGT, glycerol dialkyl glycerol tetraether; GI, Greenland Interstadial; GS, Greenland Stadial; LOI, loss on ignition; MAF, months above freezing; MAT, modern analogue technique; MIS, Marine Isotope Stage; MSL, mean sea level; NGRIP, North Greenland Ice Core Project; NH, Northern Hemisphere; OSL, optically stimulated luminescence; WA-PLS, weighted-averaging partial least squares.

References

Batchelor, C.L., Margold, M., Krapp, M., Murton, D.K., Dalton, A.S., Gibbard, P.L. et al. (2019) The configuration of Northern Hemisphere ice sheets through the Quaternary. *Nature Communications*, 10(1), 3713. Available at: https://doi.org/10.1038/s41467-019-11601-2

Behre, K.E. (1989) Biostratigraphy of the last glacial period in Europe. *Quaternary Science Reviews*, 8(1), 25–44. Available at: https://doi.org/10.1016/0277-3791(89)90019-X

Behre, K.-E., Hölzer, A. & Lemdahl, G. (2005) Botanical macroremains and insects from the Eemian and Weichselian site of Oerel (northwest Germany) and their evidence for the history of climate. *Vegetation History and Archaeobotany*, 14, 31–53.

Berger, A. (1978) Long-term Variations of Daily Insolation and Quaternary Climatic Changes. *Journal of the Atmospheric Sciences*, 35(12), 2362–2367.

Birks, H.J.B. (2003) Quantitative palaeoenvironmental reconstructions from Holocene biological data. In: Mackay, A., Battarbee, R., Birks, H.J. & O., F, (Eds.) *Global Change in the Holocene*. Arnold. pp. 107–123. https://doi.org/10.4324/9780203785027

Boyer, T.P., Antonov, J.I., Baranova, O.K. et al. (2013) WORLD OCEAN DATABASE 2013. In *Sydney Levitus, Ed.; Alexey Mishonoc, Technical Ed.; NOAA Atlas NESDIS 72*. https://doi.org/10.7289/V5NZ85MT

Brauer, A., Allen, J.R.M., Mingram, J., Dulski, P., Wulf, S. & Huntley, B. (2007) Evidence for last interglacial chronology and environmental change from Southern Europe. *Proceedings of the National Academy of Sciences of the United States of America104*, (2), 450–455. https://doi.org/10.1073/PNAS.0603321104

Bush, R.T. & McInerney, F.A. (2013) Leaf wax n-alkane distributions in and across modern plants: Implications for paleoecology and chemotaxonomy. *Geochimica et Cosmochimica Acta*, 117, 161–179. Available at: https://doi.org/10.1016/j.gca.2013.04.016

Busschers, F.S., Kasse, C., van Balen, R.T., Vandenberghe, J., Cohen, K.M., Weerts, H.J.T. et al. (2007) Late Pleistocene evolution of the Rhine-Meuse system in the southern North Sea basin: imprints of climate change, sea-level oscillation and glacio-isostacy. *Quaternary Science Reviews*, 26(25–28), 3216–3248. Available at: https://doi.org/10.1016/j.quascirev.2007.07.013

Cameron, T.D.J., Schuttenhelm, R.T.E. & Laban, C. (1989) Middle and Upper Pleistocene and Holocene stratigraphy in the southern North Sea between 52° and 54° N, 2° to 4° E. In: Henriet, J.P. & De Moor, G., (Eds.) *The Quaternary and Tertiary Geology of the Southern Bight, North Sea*. Ministry of Economic Affairs - Belgian Geological Survey. pp. 119–136.

CCKP. (2024) *Climate Change Knowledge Portal, Netherlands, Current Climate, Climatology*. https://climateknowledgeportal.worldbank.org/country/netherlands/climate-data-historical

Chevalier, M., Davis, B.A.S., Heiri, O., Seppä, H., Chase, B.M., Gajewski, K. et al. (2020) Pollen-based climate reconstruction techniques for late Quaternary studies. *Earth-Science Reviews*, 210(September), 103384. Available at: https://doi.org/10.1016/j.earscirev.2020.103384

Cleveringa, J. (2000) Reconstruction and modelling of Holocene coastal evolution of the western Netherlands. In *Geologica Ultraiectina* (Issue 200). Utrecht University.

Dalton, A.S., Stokes, C.R. & Batchelor, C.L. (2022) Evolution of the Laurentide and Innuitian ice sheets prior to the Last Glacial Maximum (115 ka to 25 ka). *Earth-Science Reviews*, 224(103875), 1–33. Available at: https://doi.org/10.1016/j.earscirev.2021.103875

Dam, H., Mertens, A. & Sinkeldam, J. (1994) A coded checklist and ecological indicator values of freshwater diatoms from the Netherlands. *Netherlands Journal of Aquatic Ecology*, 28(1), 117–133.

Damsté, J.S.S., Hopmans, E.C., Pancost, R.D., Schouten, S. & Geenevasen, J.A.J. (2000) Newly discovered non-isoprenoid glycerol dialkyl glycerol tetraether lipids in sediments. *Chemical Communications*, 17, 1683–1684. Available at: https://doi.org/10.1039/b004517i

Davis, B.A.S., Chevalier, M., Sommer, P., Carter, V.A., Finsinger, W., Mauri, A. et al. (2020) The Eurasian Modern Pollen Database (EMPD), version 2. *Earth System Science Data*, 12(4), 2423–2445. Available at: https://doi.org/10.5194/essd-12-2423-2020

Dearing Crampton-Flood, E., Peterse, F., Munsterman, D. & Sinninghe Damsté, J.S. (2018) Using tetraether lipids archived in North Sea Basin sediments to extract North Western European Pliocene continental air temperatures. *Earth and Planetary Science Letters*, 490, 193–205. Available at: https://doi.org/10.1016/J.EPSL.2018.03.030

Dearing Crampton-Flood, E., Tierney, J.E., Peterse, F., Kirkels, F.M.S.A. & Sinninghe Damsté, J.S. (2020) BayMBT: A Bayesian calibration model for branched glycerol dialkyl glycerol tetraethers in soils and peats. *Geochimica et Cosmochimica Acta*, 268, 142–159. Available at: https://doi.org/10.1016/j.gca.2019.09.043

Denys, L. (1991) A check-list of the diatoms in the Holocene deposits of the Western Belgian coastal plain with survey of their apparent ecological requirements, In *Service Geologique de Belgique: Vol. 1,2*. Belgium: Ministy of economic affairs.

Eaton, S.J., Hodgson, D.M., Barlow, N.L.M., Mortimer, E.E.J. & Mellett, C.L. (2020) Palaeogeographical changes in response to glacial–interglacial cycles, as recorded in Middle and Late Pleistocene seismic stratigraphy, southern North Sea. *Journal of Quaternary Science*, 35(6), 760–775. Available at: https://doi.org/10.1002/JQS.3230

Eglinton, G. & Hamilton, R.J. (1967) Leaf Epicuticular Waxes. *Science*, 156(3780), 1322–1335. Available at https://doi.org/10.1126/science.156.3780.1322

EMODnet Bathymetry Consortium. (2020) *European marine observation data network (EMODnet) Bathymetry*. https://emodnet.eu/bathymetry [Accessed December 2020]

Ficken, K.J., Li, B., Swain, D.L. & Eglinton, G. (2000) An n-alkane proxy for the sedimentary input of submerged/floating freshwater aquatic macrophytes. *Organic Geochemistry*, 31(7–8), 745–749. Available at: https://doi.org/10.1016/S0146-6380(00)00081-4

Gowan, E.J., Zhang, X., Khosravi, S., Rovere, A., Stocchi, P., Hughes, A.L.C. et al. (2021) A new global ice sheet reconstruction for the past 80000 years. *Nature Communications*, 12(1199), 1–9. Available at: https://doi.org/10.1038/s41467-021-21469-w

Guiot, J., Pons, A., De Beaulieu, J.L. & Reille, M. (1989) A 140,000-year continental climate reconstruction from two European pollen records. *Nature*, 338(6213), 309–313.

Hammer, Ø., Harper, D.A.T. & Ryan, P.D. (2001) PAST: Paleontological Statistics software package for education and data analysis. *Palaeontologia Electronica. Palaeontologia Electronica*, 4(1), 9.

Hijma, M.P., Cohen, K.M., Roebroeks, W., Westerhoff, W.E. & Busschers, F.S. (2012) Pleistocene Rhine–Thames landscapes:

© 2024 The Author(s). *Journal of Quaternary Science* Published by John Wiley & Sons Ltd.

geological background for hominin occupation of the southern North Sea region. *Journal of Quaternary Science*, 27(1), 17–39. Available at: https://doi.org/10.1002/JQS.1549

Hopmans, E.C., Schouten, S. & Sinninghe Damsté, J.S. (2016) The effect of improved chromatography on GDGT-based palaeoproxies. *Organic Geochemistry*, 93, 1–6. Available at: https://doi.org/10.1016/J.ORGGEOCHEM.2015.12.006

Hopmans, E.C., Weijers, J.W., Schefuß, E., Herfort, L., Damsté, J.S.S. & Schouten, S. (2004) A novel proxy for terrestrial organic matter in sediments based on branched and isoprenoid tetraether lipids. *Earth and Planetary Science Letters*, 224(1-2), 107–116.

De Jonge, C., Hopmans, E.C., Zell, C.I., Kim, J.H., Schouten, S. & Sinninghe Damsté, J.S. (2014) Occurrence and abundance of 6-methyl branched glycerol dialkyl glycerol tetraethers in soils: Implications for palaeoclimate reconstruction. *Geochimica et Cosmochimica Acta*, 141, 97–112. Available at: https://doi.org/10.1016/j.gca.2014.06.013

Juggins, S. (2007) C2 Software for ecological and palaeoecological data analysis and visualisation. User guide version 1.5. In *University of Newcastle*.

Kiden, P., Denys, L. & Johnston, P. (2002) Late Quaternary sea-level change and isostatic and tectonic land movements along the Belgian–Dutch North Sea coast: geological data and model results. *Journal of Quaternary Science*, 17(5–6), 535–546. Available at: https://doi.org/10.1002/jqs.709

Kidwell, S.M. (1986) Models for Fossil Concentrations: Paleobiologic Implications. *Paleobiology*, 12(1), 6–24.

KNMI. (2024) *Daggegevens van Noordzee stations*. https://www.knmi.nl/nederland-nu/klimatologie/daggegevens_Noordzee

Laban, C. (1995) *The Pleistocene Glaciations in the Dutch Sector of the North Sea. A Synthesis of Sedimentary and Seismic Data*. [University of Amsterdam]. https://hdl.handle.net/11245/1.119444

Laban, C. & Mesdag, C.S. (1995) *Oyster Grounds: Quaternary Geology, sheet 54 N\04E, 1:250 000 series*. Geological Survey of the Netherlands.

Lattaud, J., Dorhout, D., Schulz, H., Castañeda, I.S., Schefuß, E., Sinninghe Damsté, J.S. et al. (2017a) The C₃₂ alkane-1,15-diol as a proxy of late Quaternary riverine input in coastal margins. *Climate of the Past*, 13(8), 1049–1061. Available at: https://doi.org/10.5194/cp-13-1049-2017

Lattaud, J., Kim, J.H., De Jonge, C., Zell, C., Sinninghe Damsté, J.S. & Schouten, S. (2017b) The C32 alkane-1,15-diol as a tracer for riverine input in coastal seas. *Geochimica et Cosmochimica Acta*, 202(12), 146–158. Available at: https://doi.org/10.1016/j.gca.2016.12.030

Limpenny, S.E., Barrio Froján, C., Cotterill, C., Foster-Smith, R.L., Pearce, B., Tizzard, L. et al. (2011) The East Coast Regional Environmental Characterisation. In *Cefas Open report 08/04, MEPF*.

Lisiecki, L.E. & Raymo, M.E. (2005) A Pliocene-Pleistocene stack of 57 globally distributed benthic δ 18 O records. *Paleoceanography*, 20(1), 1–17. Available at: https://doi.org/10.1029/2004PA001071

McManus, J.F., Bond, G.C., Broecker, W.S., Johnsen, S., Labeyrie, L. & Higgins, S. (1994) High-resolution climate records from the North Atlantic during the last interglacial. *Nature*, 371(6495), 326–329.

Medina-Elizalde, M. (2013) A global compilation of coral sea-level benchmarks: Implications and new challenges. *Earth and Planetary Science Letters*, 362, 310–318. Available at: https://doi.org/10.1016/j.epsl.2012.12.001

Meijer, T., Pouwer, R., Cleveringa, P., de Wolf, H., Busschers, F.S. & Wesselingh, F.P. (2021) Fossil molluscs from the borehole Hollum (Ameland, the Netherlands) constrain three successive Quaternary interglacial marine intervals in the southern North Sea Basin. *Netherlands Journal of Geosciences*, 100(e13), 1–8. Available at: https://doi.org/10.1017/njg.2021.2

Missiaen, T., Fitch, S., Harding, R., Muru, M., Fraser, A., De Clercq, M. et al. (2021) Targeting the Mesolithic: Interdisciplinary approaches to archaeological prospection in the Brown Bank area, southern North Sea. *Quaternary International*, 584, 141–151. Available at: https://doi.org/10.1016/J.QUAINT.2020.05.004

Müller, U.C. & Sánchez Goñi, M.F. (2007) 19. Vegetation dynamics in southern Germany during marine isotope stage 5 (~130 to 70 kyr ago). *Developments in Quaternary Science*, 7(C), 277–287. Available at: https://doi.org/10.1016/S1571-0866(07)80044-3

North Greenland Ice Core Project (NGRIP) Members. (2004) High-resolution record of Northern Hemisphere climate extending into the last interglacial period. *Nature431*, (7005), 147–151. www.nature.com/nature

Oele, E. (1971) The Quaternary geology of the southern area of the Dutch part of the North Sea. *Geologie en Mijnbouw*, 50(3), 461–474.

Peeters, J., Busschers, F.S. & Stouthamer, E. (2015) Fluvial evolution of the Rhine during the last interglacial-glacial cycle in the southern North Sea basin: A review and look forward. *Quaternary International*, 357, 176–188. Available at: https://doi.org/10.1016/J.QUAINT.2014.03.024

Peterse, F., Kim, J.H., Schouten, S., Kristensen, D.K., Koç, N. & Sinninghe Damsté, J.S. (2009) Constraints on the application of the MBT/CBT palaeothermometer at high latitude environments (Svalbard, Norway). *Organic Geochemistry*, 40(6), 692–699. Available at: https://doi.org/10.1016/j.orggeochem.2009.03.004

Pico, T., Creveling, J.R. & Mitrovica, J.X. (2017) Sea-level records from the U.S. mid-Atlantic constrain Laurentide Ice Sheet extent during Marine Isotope Stage 3. *Nature Communications*, 8(May), 15612. Available at: https://doi.org/10.1038/ncomms15612

Ponel, P. (1995) Rissian, Eemian and Würmian Coleoptera assemblages from La Grande Pile (Vosges, France). *Palaeogeography, Palaeoclimatology, Palaeoecology*, 114, 1–41.

Rampen, S.W., Schouten, S., Wakeham, S.G. & Sinninghe Damsté, J.S. (2007) Seasonal and spatial variation in the sources and fluxes of long chain diols and mid-chain hydroxy methyl alkanoates in the Arabian Sea. *Organic Geochemistry*, 38(2), 165–179. Available at: https://doi.org/10.1016/J.ORGGEOCHEM.2006.10.008

Riechelmann, D.F.C., Albert, J., Britzius, S., Krebsbach, F., Scholz, D., Schenk, F. et al. (2023) Bioproductivity and vegetation changes documented in Eifel maar lake sediments (western Germany) compared with speleothem growth indicating three warm phases during the last glacial cycle. *Quaternary International*, 673, 1–17.

Rohling, E.J., Grant, K., Bolshaw, M., Roberts, A.P., Siddall, M., Hemleben, C. et al. (2009) Antarctic temperature and global sea level closely coupled over the past five glacial cycles. *Nature Geoscience*, 2(7), 500–504. Available at: https://doi.org/10.1038/ngeo557

De Rosa, M. & Gambacorta, A. (1988) The Lipids of Archaebacteria. *Progress in Lipid Research*, 27(3), 153–175.

Rousseau, D.D., Hatté, C., Duzer, D., Schevin, P., Kukla, G. & Guiot, J. (2007) 15. Estimates of temperature and precipitation variations during the Eemian interglacial: New data from the grande pile record (GP XXI). *Developments in Quaternary Science*, 7(C), 231–238. Available at: https://doi.org/10.1016/S1571-0866(07)80040-6

Le Roux, J.P. (2009) Characteristics of developing waves as a function of atmospheric conditions, water properties, fetch and duration. *Coastal Engineering*, 56(4), 479–483. Available at: https://doi.org/10.1016/j.coastaleng.2008.10.007

Ruddiman, W.F. & McIntyre, A. (1981) Oceanic mechanisms for amplification of the 23,000-year ice-volume cycle. *Science*, 212(4495), 617–627. Available at: https://doi.org/10.1126/science.212.4495.617

Du Saar, A. (1970) *Diatomeeën- en ostracodenonderzoek van de Fugro-boring P 5 B. Rapport No. 176*.

Sánchez Goñi, M.F., Bard, E., Landais, A., Rossignol, L. & D'errico, F. (2013) Air-sea temperature decoupling in western Europe during the last interglacial-glacial transition. *Nature Geoscience*, 6(10), 837–841. Available at: https://doi.org/10.1038/ngeo1924

Sánchez Goñi, M.F., Loutre, M.F., Crucifix, M., Peyron, O., Santos, L., Duprat, J. et al. (2005) Increasing vegetation and climate gradient in Western Europe over the Last Glacial Inception (122-110 ka): Data-model comparison. *Earth and Planetary Science Letters*, 231(1–2), 111–130. Available at: https://doi.org/10.1016/j.epsl.2004.12.010

Sejrup, H.P. & Larsen, E. (1991) Eemian-Early Weichselian N-S Temperature gradients; North Atlantic-NW Europe. *Quaternary International*, 10-12, 161–166.

Shackleton, N.J. (1969) The last interglacial in the marine and terrestrial records. *Proceedings of the Royal Society of London. Series B: Biological Sciences*, 174(1034), 135–154.

Shackleton, N.J., Sánchez-Goñi, M.F., Pailler, D. & Lancelot, Y. (2003) Marine isotope substage 5e and the Eemian interglacial. *Global and Planetary Change*, 36(3), 151–155. Available at: https://doi.org/10.1016/S0921-8181(02)00181-9

Sier, M.J., Roebroeks, W., Bakels, C.C., Dekkers, M.J., Brühl, E., De Loecker, D. et al. (2011) Direct terrestrial-marine correlation demonstrates surprisingly late onset of the last interglacial in central

© 2024 The Author(s). *Journal of Quaternary Science* Published by John Wiley & Sons Ltd.

Europe. *Quaternary Research*, 75(1), 213–218. Available at: https://doi.org/10.1016/j.yqres.2010.11.003

Sinninghe Damsté, J.S. (2016) Spatial heterogeneity of sources of branched tetraethers in shelf systems: The geochemistry of tetraethers in the Berau River delta (Kalimantan, Indonesia. *Geochimica et Cosmochimica Acta*, 186, 13–31. Available at: https://doi.org/10.1016/J.GCA.2016.04.033

Sinninghe Damsté, J.S., Schouten, S., Hopmans, E.C., Van Duin, A.C., & Geenevasen, J.A. (2002). Crenarchaeol. *Journal of Lipid Research*, 43(10), 1641-1651.

Spratt, R.M. & Lisiecki, L.E. (2016) A Late Pleistocene sea level stack. *Climate of the Past*, 12(4), 1079–1092. Available at: https://doi.org/10.5194/cp-12-1079-2016

Törnqvist, T.E., Wallinga, J., Murray, A.S., De Wolf, H., Cleveringa, P. & De Gans, W. (2000) Response of the Rhine-Meuse system (west-central Netherlands) to the last Quaternary glacio-eustatic cycles: a first assessment. *Global and Planetary Change*, 27(1–4), 89–111. Available at: https://doi.org/10.1016/S0921-8181(01)00072-8

Toucanne, S., Rodrigues, T., Menot, G., Soulet, G., Cheron, S., Billy, I. et al. (2023) Marine Isotope Stage 4 (71–57 ka) on the Western European margin: Insights to the drainage and dynamics of the Western European Ice Sheet. *Global and Planetary Change, 229*(August). https://doi.org/10.1016/j.gloplacha.2023.104221

Van der Valk, L. (1992) *Mid- and late-holocene coastal evolution in the beach-barrier area of the Western Netherlands*, 45. Vrije Univeristeit Amsterdam

Volkman, J.K., Barrett, S.M., Dunstan, G.A. & Jeffrey, S.W. (1992) C30-C32 alkyl diols and unsaturated alcohols in microalgae of the class Eustigmatophyceae. *Organic Geochemistry*, 18(1), 131–138. Available at: https://doi.org/10.1016/0146-6380(92)90150-V

Vos, P.C. & de Wolf, H. (1993) Diatoms as a tool for reconstructing sedimentary environments in coastal wetlands; methodological aspects. *Hydrobiologia*, 269–270, 285–296.

Waajen, I.M., Busschers, F.S., Donders, T.H., van Heteren, S., Plets, R., Wallinga, J. et al. (2024) Late MIS5a in the southern North Sea: new chronostratigraphic insights from the Brown Bank Formation. *Journal of Quaternary Science*, 39(3), 408–420. Available at: https://doi.org/10.1002/jqs.3592

Waelbroeck, C., Labeyrie, L., Michel, E., Duplessy, J.C., McManus, J.F., Lambeck, K. et al. (2002) Sea-level and deep water temperature changes derived from benthic foraminifera isotopic records. *Quaternary Science Reviews*, 21(1–3), 295–305. Available at: https://doi.org/10.1016/S0277-3791(01)00101-9

Weijers, J.W.H., Schouten, S., van den Donker, J.C., Hopmans, E.C. & Sinninghe Damsté, J.S. (2007) Environmental controls on bacterial tetraether membrane lipid distribution in soils. *Geochimica et Cosmochimica Acta*, 71(3), 703–713. Available at: https://doi.org/10.1016/J.GCA.2006.10.003

Weiss, T.L., Linsley, B.K., Gordon, A.L., Rosenthal, Y. & Dannenmann-Di Palma, S. (2022) Constraints on Marine Isotope Stage 3 and 5 Sea Level From the Flooding History of the Karimata Strait in Indonesia. *Paleoceanography and Paleoclimatology*, 37(9), e2021PA004361. Available at: https://doi.org/10.1029/2021PA004361

Van der Werf, J.J., Grasmeijer, B., Hendriks, E., Van der Spek, A.J.F. & Vermaas, T. (2017) *Literature study Dutch lower shoreface*.

Wessex Archaeology. (2018) *Norfolk Vanguard Offshore Wind Farm Stage 3 Geoarchaeological Sampling and Assessment* (Issue March). https://corporate.vattenfall.co.uk/globalassets/uk/projects/norfolk-vanguard/en010079-000022-scoping-report-6.pdf

Wohlfarth, B. (2013) *A review of Early Weichselian climate (MIS 5d-a) in Europe*. Technical report/Svensk kärnbränslehantering AB.

Woillard, G.M. (1978) Grande Pile peat bog: A continuous pollen record for the last 140,000 years. *Quaternary Research*, 9(1), 1–21. Available at: https://doi.org/10.1016/0033-5894(78)90079-0

Wolff, E.W., Chappellaz, J., Blunier, T., Rasmussen, S.O. & Svensson, A. (2010) Millennial-scale variability during the last glacial: The ice core record. *Quaternary Science Reviews*, 29(21–22), 2828–2838. Available at: https://doi.org/10.1016/j.quascirev.2009.10.013

Zagwijn, W.H. (1983) Sea-level changes in the Netherlands during the Eemian. *Geologie en Mijnbouw*, 62, 437–450.

Ziemann, H. (1971) Die Wirkung des Salzgehaltes auf die Diatomeenflora als Grundlage für eine biologische Analyse und Klassifikation der Binnengewässer. *Limnologica*, 8, 505–525.

© 2024 The Author(s). *Journal of Quaternary Science* Published by John Wiley & Sons Ltd.